# Amplitude squeezing in a semiconductor laser using quantum nondemolition measurement and negative feedback

Y. Yamamoto, N. Imoto, and S. Machida
*Musashino Electrical Communication Laboratories, Nippon Telegraph and Telephone Corporation, Musashino-shi, Tokyo 180, Japan*
(Received 16 September 1985)

A new scheme for generating an amplitude-squeezed state is proposed. The photon-flux fluctuation of a semiconductor-laser output wave is measured with a quantum nondemolition (QND) detector, and is negatively fed back to the laser pumping current. The operator Langevin equations are derived by combining the quantum-mechanical analyses on the laser internal-external field fluctuations, the quantum nondemolition detector based on an optical Kerr effect, and a negative-feedback circuit. The output wave features a reduced photon number noise below the standard quantum limit, $\langle(\Delta\hat{n})^2\rangle < \langle\hat{n}\rangle$, and an enhanced phase noise above that, $\langle(\Delta\hat{\psi})^2\rangle > \frac{1}{4}\langle\hat{n}\rangle^{-1}$, while the minimum uncertainty product is still preserved. The observed photoelectron statistics in a negative-feedback GaAs laser diode using a conventional *p-i-n* photodiode (not a QND detector) are shown to exhibit sub-Poissonian statistics with the variance $\langle(\Delta\hat{n})^2\rangle \cong 0.26\langle\hat{n}\rangle$. The measured photocurrent fluctuation spectral density is also indicated to be below the standard quantum limit by a factor of 0.2 ($=-7$ dB). The experimental results also confirm that such amplitude squeezing is only observed inside the feedback loop and cannot be extracted from the loop unless a quantum nondemolition detector is used.

## I. INTRODUCTION

Recently, considerable interest has surfaced in the nonclassical properties of particular photon states. There are three typical quantum effects which represent the characteristics of these nonclassical photons. The first is squeezing in which the uncertainties $\Delta\hat{a}_1$ and $\Delta\hat{a}_2$ in the two quadrature components of the field amplitude are different while the product satisfies the minimum uncertainty relationship $\langle(\Delta\hat{a}_1)^2\rangle\langle(\Delta\hat{a}_2)^2\rangle = \frac{1}{16}$. The second is the sub-Poissonian photon statistics in which the photon statistics $P(n)$ is narrower than the Poisson distribution. The third is photon antibunching wherein the second-order intensity correlation function $\langle I(t)I(t-\tau)\rangle$ has a minimal value of $\tau=0$.

Figure 1 shows the uncertainty in the $a_1$-$a_2$ space for several photon states. Here, $a_1$ is the cosine quadrature and $a_2$ is the sine quadrature of the optical wave. Figure 1(a) represents the Glauber coherent state, which is referred to as a "classical state," while Figs. 1(b)–1(g) are nonclassical states.

The quantum-mechanical representation and properties of a squeezed state (or a two-photon coherent state) have been extensively studied.[1–3] Two special cases of squeezed states are shown in Figs. 1(b) and 1(c). An "in-phase squeezed state" involves the reduced quantum noise along the direction of coherent excitation, which exhibits sub-Poissonian photon statistics and photon antibunching as well as squeezing. A "quadrature squeezed state" features reduced quantum noise in quadrature to the coherent excitation, which exhibits squeezing only. The limiting cases of zero and infinite quantum noise in two quadratures have been referred to as a "quadrature phase eigenstate"[4,5] and are shown in Figs. 1(e) and 1(f). Also discussed has been improvement of the signal-to-noise ratio in optical communications[6–8] and of optical-interferometer gravitational-wave detectors[9,10] using a squeezed state.

The current interest in a squeezed state is now focused on generating it and observing its characteristic quantum effects. Several schemes have been suggested to generate a

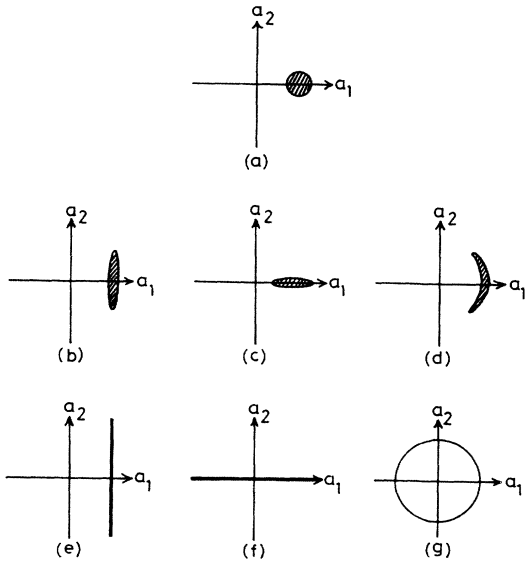


FIG. 1. The uncertainty in $a_1$(cosine)-$a_2$(sine) space for typical photon states: (a) coherent state, (b) in phase-squeezed state, (c) quadrature-squeezed state, (d) amplitude-squeezed state, (e),(f) quadrature phase eigenstates, and (g) number state.

 

squeezed state such as a degenerate parametric amplifier,[1] a degenerate four-wave mixer,[11,12] a cavity degenerate four-wave mixer,[13] nondegenerate four-wave mixing in a single-mode fiber,[14] and other various nonlinear optical processes. An extensive review on the squeezed state is given in Ref. 15.

Although an in-phase squeezed state exhibits sub-Poissonian photon statistics, the deviation from a Poisson distribution is not large. This is because the enhanced noise in the $a_2$ quadrature component gives rise to the increased photon number noise. The minimum photon number variance of the in-phase squeezed state is calculated[10] to be $\langle(\Delta\hat{n})^2\rangle \simeq \langle\hat{n}\rangle^{2/3}$. A photon number eigenstate, on the other hand, has zero uncertainty for the photon number as shown in Fig. 1(g). As the quadrature phase eigenstates represent the extreme cases of an in-phase squeezed state and a quadrature squeezed state, a photon number eigenstate is indicative of the extreme case of an "amplitude squeezed state" shown in Fig. 1(d). Such an amplitude-squeezed state features a reduced photon number noise $\langle(\Delta\hat{n})^2\rangle < \langle\hat{n}\rangle$ and an enhanced phase noise $\langle(\Delta\hat{\phi})^2\rangle > \frac{1}{4}\langle\hat{n}\rangle^{-1}$, in which the minimum uncertainty relationship $\langle(\Delta\hat{n})^2\rangle\langle(\Delta\hat{\phi})^2\rangle \simeq \frac{1}{4}$ is still preserved. This is essentially the nonclassical photon state we will discuss in this paper. The mathematical description of the minimum uncertainty states for $\Delta\hat{n}$ and $\Delta\hat{\phi}$ is extensively discussed in Ref. 16.

Photon antibunching and sub-Poissonian photon statistics were observed in a resonant fluorescence.[17] Sub-Poissonian photon statistics were also observed in a Frank-Hertz light.[18] However, these lights are essentially incoherent both spatially and temporally. The available optical power and deviation from a Poisson distribution are also weak.

In this paper we propose a new scheme which generates an (intense and coherent) amplitude squeezed state. The scheme is composed of a diode laser, the quantum nondemolition (QND) detector for photon-flux measurement and a negative-feedback circuit.[19] The photon-flux fluctuation measured by a QND detector is negatively fed back to a laser pumping current. The temporal fluctuation of the output photon flux is analyzed using quantum-mechanical Langevin equations. The obtained noise power spectrum is shown to be reduced below the standard quantum noise level of a coherent state, that is, the shot noise level. A preliminary experiment of a feedback GaAs laser using a conventional photodetector instead of a QND measurement scheme is also presented. The experimental results indicate that not only excess noise but also quantum noise can be suppressed inside the feedback loop as is predicted by the theory. Furthermore, the noise of the output wave extracted from the feedback loop by a half-mirror is shown to increase unless the QND measurement scheme is used.

The proposed scheme is based on two important assumptions. One is that "negative feedback" does not introduce a new quantum noise source. This assumption is theoretically supported by the fact that the commutation relationship for a photon operator in a negative-feedback laser is properly preserved without introducing an additional noise operator.[20] The experimental results described in this paper also support this assumption. The other assumption is that our QND detector can measure photon-flux fluctuation with arbitrarily high accuracy without introducing any disturbance into the photon flux. It has been proved that this is possible using an optical Kerr effect.[21]

The basic conception of the proposed scheme is described in Sec. II. In Sec. III we offer a theoretical analysis using the classical equation of motion for an open cavity, which relates an incident wave, internal field, and reflected wave. This equation is extended to an operator equation by introducing a zero-point fluctuation (quantum noise of a vacuum state) to an incident wave. The equation is further extended to quantum-mechanical Langevin equations for a semiconductor laser by introducing the interaction with the two reservoirs: the inverted electronic systems of continuous bands and the distributed loss oscillators which account for internal loss. The resulting equations are equivalent to the conventional Langevin equations[22–24] insofar as only internal field fluctuation is considered. They are different, however, from the conventional ones as external output-wave fluctuations can also be obtained by them.

The amplitude and phase fluctuation spectra for an internal field and an output wave of a free-running semiconductor laser are obtained in Sec. IV. The measurement accuracy of a photon flux and the additional phase noise imposed on the laser output wave in the quantum nondemolition detector based on an optical Kerr medium are discussed in Sec. V. The final formulas of operator Langevin equations are derived in Sec. VI by combining these analyses for the purpose of describing the entire system. Here, the reduced photon-flux fluctuation spectrum and enhanced phase fluctuation spectrum are obtained. It is shown that an output wave of the entire system is in an amplitude-squeezed state which satisfies the number-phase minimum uncertainty product.

The experimental results are delineated in Secs. VII and VIII. The experimental calibration of the standard quantum noise level and Poissonian photon statistics was accomplished using a light-emitting diode. The photocurrent fluctuation spectrum and photoelectron statistics in the feedback semiconductor laser were compared with the standard quantum limit. The photocurrent fluctuation spectrum was reduced below the standard quantum limit by a factor of 0.2 ($-7$ dB) and sub-Poissonian photoelectron statistics having $\langle(\Delta\hat{n})^2\rangle \cong 0.26\langle\hat{n}\rangle$ were observed.

In the final section (Sec. IX) we will discuss the implication of the proposed scheme from the viewpoint of reduction of wave function by QND measurement and quantum state preparation.

## II. BASIC SCHEME CONCEPTUALIZATION AND SUMMARY OF ANALYSIS

The basic conception of the proposed scheme involves the semiconductor-laser photon-flux stabilization by a negative-feedback loop, in which the photon-flux fluctuation of a semiconductor-laser output wave is measured

without disturbing it using a quantum nondemolition measurement. The configuration of the scheme is detailed in Fig. 2. A semiconductor laser is used as a laser oscillator, because its output-wave photon flux is easily controlled through an electrical pumping current. The bandwidth of a feedback loop can be considerably broader due to the high-frequency modulation capability and the small size of a semiconductor laser.

The semiconductor-laser internal field $\hat{a}$ is extracted through a partially reflecting mirror, $R' < 1$, as an output wave $\hat{r}_1$. Wave $\hat{r}_1$ passes through a transparent optical Kerr medium and modulates the medium refractive index according to its photon flux $\hat{N}(t)$. The refractive-index modulation can be measured by a probe wave $\hat{r}_p$. The phase retardation of the probe wave encountered in the Kerr medium is a function of the medium refractive-index modulation and thus optical phase detection such as optical homodyning can read out the laser output-wave photon flux $\hat{N}(t)$ without disturbing it.

The electrical current of the optical phase detector, $\hat{i}(t)$, is proportional to photon flux $\hat{N}(t)$ and is compared with a dc bias current $i_0$. The difference between the two currents is then negatively fed back to the semiconductor-laser injection current to eliminate it. The output-wave photon flux $\hat{N}(t)$ does not change in an optical Kerr medium, and, therefore, the output wave $\hat{r}_2$ has the same photon flux, that is, $\hat{N}_{r_2}(t) = \hat{N}_{r_1}(t)$.

When the feedback loop has a very large gain, the error signal $\Delta\hat{i}(t)$, which represents the difference between the dc bias current and the QND output current, can be reduced to an arbitrarily small value. This means the output-wave photon-flux fluctuation can be suppressed arbitrarily if the measurement uncertainty of the QND detector is negligible.

There are four main conclusions we will show in this paper. First, the negative feedback can reduce not only classical noise (excess noise) but also quantum noise. Second, the theoretical limit on the photon-flux noise reduction is imposed by the phase noise $\Delta\hat{\phi}_p$ of a probe wave used in QND measurement because it determines the measurement uncertainty of the QND detector. Third, the phase noise $\Delta\hat{\phi}_p$ can be reduced by increasing the probe wave photon number according to $\langle(\Delta\hat{\phi}_p)^2\rangle = \frac{1}{4}\langle\hat{n}_p\rangle^{-1}$. This results in the increased probe wave photon number noise $\langle(\Delta\hat{n}_p)^2\rangle = \langle\hat{n}_p\rangle$, which modulates the laser output-wave phase $\hat{\psi}$ more randomly via the optical Kerr effect and enhances the phase noise. Fourth, this back action of the QND detection on the laser output-wave phase ensures that the minimum uncertainty product $\langle(\Delta\hat{n})^2\rangle\langle(\Delta\hat{\psi})^2\rangle = \frac{1}{4}$ is preserved. That is, the photon number noise is reduced below the standard quantum limit, $\langle(\Delta\hat{n})^2\rangle < \langle\hat{n}\rangle$, and the phase noise is enhanced above it, $\langle(\Delta\hat{\psi})^2\rangle > \frac{1}{4}\langle\hat{n}\rangle^{-1}$. The amplitude-squeezed state shown in Fig. 1(d) is thus generated by the present scheme.

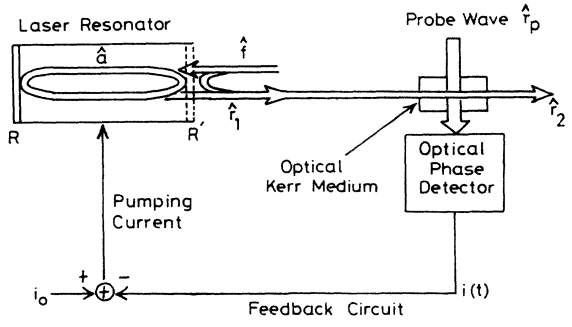


FIG. 2. Configuration for the proposed scheme, which contains a laser oscillator, a QND detector for the optical intensity, and a negative-feedback circuit for the injection current.

## III. QUANTUM-MECHANICAL LANGEVIN EQUATIONS FOR A SEMICONDUCTOR-LASER INTERNAL FIELD AND OUTPUT WAVE

There are several ways to express the quantum-mechanical states of a photon field. The representation by the number state expansion[16] and by Yuen's $Q$ function[3] are complete descriptions for any photon state. The Glauber-Sudarshan $P(\alpha)$ representation,[25,26] on the other hand, does not exist as an analytic function for some quantum states such as squeezed states or number states. The simplest parameter for describing the nonclassical behavior of an amplitude-squeezed state may be the photon number variance, or, in other words, the second moment of the photon distributions, $\langle(\Delta\hat{n})^2\rangle \equiv \langle(\hat{n} - \langle\hat{n}\rangle)^2\rangle$, and the phase variance, $\langle(\Delta\hat{\phi})^2\rangle$. Here, one can use $\langle(\Delta\hat{n})^2\rangle$ to tell whether or not the generated state has a smaller photon number uncertainty than a coherent state.

In the present analysis, we adopt Langevin's method, which treats the temporal noise of the field or photon number rather than its ensemble variance to express the nonclassical behavior. One reason we use Langevin's method is that the information we need in the end is the noise power spectrum and the variance of the output wave, which can be easily analyzed by this method. Another reason is that it is difficult to assign a density operator for a mode supported by the entire system shown in Fig. 2 including a semiconductor laser, an optical Kerr medium, and electrical feedback circuit. In the conventional quantum theory of a laser, an outer space is treated as a reservoir and can be eliminated from the equation of motion for the system of interest (internal field). In our case, the output wave constitutes part of the entire system. Langevin's method is suitable for such a case, because it can handle the continuous Fourier spectral analysis quite naturally. The quantum Langevin theory in which the external fields are not eliminated from the dynamics has been recently discussed in Ref. 27.

This section reviews the quasilinearized Langevin equations for the amplitude and phase operator of the cavity internal field and the carrier number operator. These Langevin equations are driven by three noise operators: that due to the internal optical loss and gain, that due to the external field coupled through the cavity output mirror, and that due to the dissipation of the dipole moment. The correlation functions for these Langevin noise opera-

tors are also delineated.

The classical equation of motion for the internal field $a$ in an empty cavity driven by the incident wave $f$ is[28]

$$\frac{d}{dt}a=-\frac{1}{2}\frac{\omega}{Q_e}a+\sqrt{\omega/Q_e}f\ . \tag{3.1}$$

Output wave $r_1$ is related to internal field $a$ and incident wave $f$ as[28]

$$r_1=-f+\sqrt{\omega/Q_e}a\ . \tag{3.2}$$

Here, $(\omega/Q_e)^{-1}$ is a photon lifetime due to output coupling through mirror $R'$. The relations (3.1) and (3.2) are obtained either by the time-reversal theorem,[28] by a direct analysis of multireflection for waves bouncing back and forth,[29] or by Kirchhoff's current law for an electrical circuit equivalent to a laser.[30] The laser internal field $a$ is normalized such that $|a|^2$ expresses a photon number (energy) in a laser cavity mode, while $|f|^2$ and $|r_1|^2$ express the photon flux (power) of the traveling wave. Quantization of the basic equations, (3.1) and (3.2), requires that the bosonic mode commutation relations be preserved. The internal field operator, denoted by $\hat{a}$, satisfies

$$[\hat{a}(t),\hat{a}^{\dagger}(t)]=1\ . \tag{3.3}$$

This imposes the correlation functions (Refs. 23, Chap. XIX)

$$\langle\hat{f}^{\dagger}(t)\hat{f}(u)\rangle=\delta(t-u)n_{\rm th} \tag{3.4}$$

and

$$\langle\hat{f}(t)\hat{f}^{\dagger}(u)\rangle=\delta(t-u)(1+n_{\rm th})\ , \tag{3.5}$$

where

$$n_{\rm th}=[\exp(\hbar\omega/k_BT)-1]^{-1}\ . \tag{3.6}$$

Note that operators $\hat{a}$ and $\hat{f}$ are slowly varying operators, which correspond, respectively, to $A$ and $F$ in Ref. 23.

Next we introduce the interaction of the internal field $\hat{a}$ and the electron systems, which have inverted populations caused by a pumping. The procedure for obtaining a conventional operator Langevin equation[31–34] results in

$$\begin{aligned}\frac{d}{dt}\hat{a}(t)=&-\frac{1}{2}\left[\frac{\omega}{Q_e}+\frac{\omega}{Q_0}+2i(\omega_0-\omega)\right]\hat{a}(t)\\&+\sum_{k,k'}\frac{|g_{kk'}|^2(\tilde{n}_{kC}-\tilde{n}_{k'V})}{i(\epsilon_{kk'}-\omega)+\gamma_{kk'}}\hat{a}(t)\\&-i\sum_{k,k'}\frac{g_{kk'}\tilde{F}^{\dagger}_{kCk'V}(t)}{i(\epsilon_{kk'}-\omega)+\gamma_{kk'}}+\hat{F}(t)\\&+\sqrt{\omega/Q_e}\hat{f}(t)\ ,\end{aligned} \tag{3.7}$$

where $\omega$ is the laser oscillation frequency; $\omega_0$ the cavity mode frequency; $Q_0$ the $Q$ value for photon decay due to cavity internal loss; $g_{kk'}$ the optical matrix element between electronic states $(k,C)$ and $(k',V)$ ($k$ or $k'$ means the wave number and $C$ and $V$ mean conduction and valence bands, respectively); $\tilde{n}_{kC}$ the electron number operator in $(k,C)$ $(=\tilde{b}^{\dagger}_{kC}\tilde{b}_{kC})$; $\tilde{n}_{k'V}$ the electron number operator in $(k',V)$ $(=\tilde{b}^{\dagger}_{k'V}\tilde{b}_{k'V})$; $\epsilon_{kk'}$ the frequency between $(k,C)$ and $(k',V)$; $\gamma_{kk'}$ the phase decay constant for a dipole moment; $\tilde{F}_{kCk'V}(t)$ the Langevin noise operator for a quantum-mechanical dipole moment operator, $\tilde{b}^{\dagger}_{kC}\tilde{b}_{k'V}$, dissipation process; and $\hat{F}(t)$ is the Langevin noise operator for the internal field due to the quantum-mechanical internal loss process.

We use a caret and a tilde to denote, respectively, operators for the photon field and electrons. The dipole moment operator $\tilde{b}^{\dagger}_{kC}\tilde{b}_{k'V}$ was adiabatically eliminated using the relation

$$\frac{d}{dt}\langle\tilde{b}^{\dagger}_{kC}\tilde{b}_{k'V}\rangle\ll\gamma_{kk'}\langle\tilde{b}^{\dagger}_{kC}\tilde{b}_{k'V}\rangle\ . \tag{3.8}$$

Equation (3.7) can be rewritten as

$$\begin{aligned}\frac{d}{dt}\hat{a}(t)=&-\frac{1}{2}\left[\frac{\omega}{Q_e}+\frac{\omega}{Q_0}+2i(\omega_0-\omega)\right.\\&\left.-\frac{\omega}{\mu^2}(\tilde{\chi}_i-i\tilde{\chi}_r)\right]\hat{a}(t)\\&+\hat{G}(t)+\sqrt{\omega/Q_e}\hat{f}(t)\ ,\end{aligned} \tag{3.9}$$

where substitutions

$$-i\sum_{k,k'}\frac{g_{kk'}\tilde{F}^{\dagger}_{kCk'V}(t)}{i(\epsilon_{kk'}-\omega)+\gamma_{kk'}}+\hat{F}(t)\rightarrow\hat{G}(t) \tag{3.10}$$

and

$$\sum_{k,k'}\frac{|g_{kk'}|^2(\tilde{n}_{kC}-\tilde{n}_{k'V})}{i(\epsilon_{kk'}-\omega)+\gamma_{kk'}}\rightarrow\frac{\omega}{\mu^2}(\tilde{\chi}_i-i\tilde{\chi}_r) \tag{3.11}$$

are used. Here, $\mu$ is the nonresonant refractive index and $\tilde{\chi}_i$ is the photon gain operator. Using the stimulated emission rate $\tilde{E}_{CV}$ and the absorption rate $\tilde{E}_{VC}$, $\tilde{\chi}_i$ is expressed as

$$\frac{\omega}{\mu^2}\tilde{\chi}_i=\tilde{E}_{CV}-\tilde{E}_{VC}\ , \tag{3.12}$$

where

$$\tilde{E}_{CV}=\sum_{k,k'}\frac{|g_{kk'}|^2\gamma_{kk'}\tilde{n}_{kC}(1-\tilde{n}_{k'V})}{(\epsilon_{kk'}-\omega)^2+\gamma^2_{kk'}} \tag{3.13}$$

and

$$\tilde{E}_{VC}=\sum_{k,k'}\frac{|g_{kk'}|^2\gamma_{kk'}(1-\tilde{n}_{kC})\tilde{n}_{k'V}}{(\epsilon_{kk'}-\omega)^2+\gamma^2_{kk'}}\ . \tag{3.14}$$

The electron system is described by one equation for a total conduction electron number $\tilde{N}_c=\sum_k\tilde{n}_{kC}$ because the intraband electron relaxation rate is very fast and the conduction electron can be assumed to be always in a quasi-Fermi-Dirac distribution. The equation of motion for $\tilde{N}_c$ is

$$\frac{d}{dt}\tilde{N}_c(t)=p-\frac{\tilde{N}_c(t)}{\tau_{\rm sp}}-\frac{\omega}{\mu^2}\tilde{\chi}_i\hat{n}(t)-\tilde{E}_{CV}+\tilde{F}_c(t)\ , \tag{3.15}$$

where $p$ is the pumping rate, $\tau_{sp}$ the spontaneous carrier lifetime, $\hat{n}(t)$ the photon number operator $[=\hat{a}^{\dagger}(t)\hat{a}(t)]$, and $\tilde{F}_c(t)$ is the Langevin noise operator for quantum-mechanical pumping, spontaneous emission, and dipole moment dissipation processes.

Our goal in this section is to obtain quasilinearized operator Langevin equations (3.24)–(3.26) from (3.9) and (3.15). In the approximation of a large photon number, we can introduce a quasilinearization to express $\hat{a}(t)$ and $\tilde{N}_c(t)$ as

$$\hat{a}(t)=[A_0+\Delta\hat{A}(t)]\exp[-i\,\Delta\hat{\phi}(t)]\ , \tag{3.16}$$

$$\tilde{N}_c(t)=N_{c0}+\Delta\tilde{N}_c(t)\ , \tag{3.17}$$

$$\tilde{\chi}_i\simeq\langle\tilde{\chi}_i\rangle+\frac{d\langle\tilde{\chi}_i\rangle}{dN_{c0}}\Delta\tilde{N}_c\ , \tag{3.18}$$

$$\tilde{\chi}_r\simeq\langle\tilde{\chi}_r\rangle+\frac{d\langle\tilde{\chi}_r\rangle}{dN_{c0}}\Delta\tilde{N}_c\ , \tag{3.19}$$

and

$$\hat{n}=[A_0+\Delta\hat{A}(t)]^2\simeq A_0^2+2A_0\,\Delta\hat{A}(t)\ , \tag{3.20}$$

where $A_0$ and $N_{c0}$ are, respectively, the expectation values (positive real) for $\hat{a}$ and $\tilde{N}_c$, and only the first-order fluctuation contributions are left in (3.18)–(3.20). Furthermore, we introduce the following notations:

$$\frac{1}{\tau_{st}}\equiv\frac{\omega}{\mu^2}\frac{d\langle\tilde{\chi}_i\rangle}{dN_{c0}}A_0^2\ , \tag{3.21}$$

$$\alpha\equiv\frac{d\langle\tilde{\chi}_r\rangle}{dN_{c0}}\Big/\frac{d\langle\tilde{\chi}_i\rangle}{dN_{c0}}\ , \tag{3.22}$$

and

$$\frac{1}{\tau_{ph}}\equiv\frac{\omega}{Q_e}+\frac{\omega}{Q_0}\ . \tag{3.23}$$

Here, $\tau_{st}$ is the stimulated emission carrier lifetime, $\alpha$ is the so-called detuning parameter or linewidth-enhancement factor,[24,35] and $\tau_{ph}$ is the photon lifetime.

Using (3.16)–(3.23) and (3.12), Langevin equations (3.9) and (3.15) are rewritten as

$$\frac{d}{dt}\Delta\hat{A}=\frac{1}{2A_0\tau_{st}}\Delta\tilde{N}_c+\hat{H}_r(t)\ , \tag{3.24}$$

$$\frac{d}{dt}\Delta\hat{\phi}=\frac{\alpha}{2A_0^2\tau_{st}}\Delta\tilde{N}_c+\frac{1}{A_0}\hat{H}_i(t)\ , \tag{3.25}$$

and

$$\frac{d}{dt}\Delta\tilde{N}_c=-\left[\frac{1}{\tau_{sp}}+\frac{1}{\tau_{st}}\right]\Delta\tilde{N}_c-\frac{2A_0}{\tau_{ph}}\Delta\hat{A}+\tilde{F}_c\ , \tag{3.26}$$

where $\hat{H}_r(t)$ and $\hat{H}_i(t)$ are Hermitian noise operators defined as

$$\hat{H}_r(t)=\tfrac{1}{2}[\hat{G}(t)+\sqrt{\omega/Q_e}\hat{f}(t)]e^{i\Delta\hat{\phi}}+\tfrac{1}{2}e^{-i\Delta\hat{\phi}}[\hat{G}^{\dagger}(t)+\sqrt{\omega/Q_e}\hat{f}^{\dagger}(t)]\ , \tag{3.27}$$

and

$$\hat{H}_i(t)=\frac{i}{2}[\hat{G}(t)+\sqrt{\omega/Q_e}\hat{f}(t)]e^{i\Delta\hat{\phi}}-\frac{i}{2}e^{-i\Delta\hat{\phi}}[\hat{G}^{\dagger}(t)+\sqrt{\omega/Q_e}\hat{f}^{\dagger}(t)]\ . \tag{3.28}$$

The detailed derivation of these equations is described in Appendix A. The correlation functions of $\hat{H}_r(t)$ and $\hat{H}_i(t)$ are obtained from the fluctuation-dissipation theorem[23] as

$$\langle\hat{H}_r(t)\hat{H}_r(u)\rangle=\langle\hat{H}_i(t)\hat{H}_i(u)\rangle=\delta(t-u)\left[\frac{1}{2}\left[\frac{\omega}{Q_e}+\frac{\omega}{Q_0}\right](n_{th}+\tfrac{1}{2})+\tfrac{1}{4}(\langle\tilde{E}_{CV}\rangle+\langle\tilde{E}_{VC}\rangle)\right]\ . \tag{3.29}$$

The correlation function for the noise operator $\tilde{F}_c(t)$ is similarly given by

$$\langle\tilde{F}_c(t)F_c(u)\rangle=\delta(t-u)\left[p+\frac{N_{c0}}{\tau_{sp}}+\langle\tilde{E}_{CV}\rangle(A_0^2+1)+\langle\tilde{E}_{VC}\rangle A_0^2\right]\ . \tag{3.30}$$

The mutual correlation functions are

$$\langle\tilde{F}_c(t)\hat{H}_r(u)\rangle=-\delta(t-u)\tfrac{1}{2}A_0(\langle\tilde{E}_{CV}\rangle+\langle\tilde{E}_{VC}\rangle) \tag{3.31}$$

and

$$\langle\tilde{F}_c(t)\hat{H}_i(t)\rangle=0\ . \tag{3.32}$$

Equations (3.24)–(3.26) are the Langevin equations for the internal field amplitude and phase fluctuations and the carrier number fluctuations driven by the Langevin noise sources whose correlation functions are given by (3.29)–(3.32).

## IV. STANDARD QUANTUM LIMIT FOR AMPLITUDE AND PHASE NOISE OF A LASER OSCILLATOR

This section first reviews the noise power spectra of the internal field amplitude and phase based on the Langevin equations obtained in the previous section. Then we obtain the noise power spectra of the output-wave amplitude and phase using the relation between the internal field and the output wave [Eq. (3.2)].

Fourier analysis of Eqs. (3.24)–(3.32) provides the noise power spectrum of the internal amplitude. For the limit of a high pumping level, we obtain (Appendix B)

$$P_{\Delta\hat{A}}(\Omega)=\frac{\omega}{Q}\Big/\left[\Omega^2+\left[\frac{\omega}{Q}\right]^2\right]\ , \tag{4.1}$$

where

$$\frac{\omega}{Q}\equiv\frac{\omega}{Q_e}+\frac{\omega}{Q_0}=\frac{1}{\tau_{ph}}\ , \tag{4.2}$$

and $P$ is defined as the single-sided power spectral density per unit cps. For the derivation of (4.1), described in Ap-

pendix B, we assumed

$$\tau_{sp},\tau_{ph} \gg \tau_{st} , \tag{4.3}$$

$$A_0^2/\tau_{ph} \gg N_{c0}/\tau_{sp} , \tag{4.4}$$

and

$$\Omega \ll |A_1| . \tag{4.5}$$

The first inequality of (4.3) means that an emitted photon stays inside the cavity considerably longer than the time within which the stimulated emission process takes place and that the stimulated emission predominates over the spontaneous emission. The second inequality means that almost all photons emitted from the laser cavity are due to the stimulated emission process rather than the spontaneous process. Inequality (4.5) means that we need to consider only the frequency region below $1/\tau_{st}$. These conditions are all satisfied if a pumping level is much higher than the threshold. The thermal photon number $n_{th}$, extremely small compared with unity for the optical frequency region at room temperature, is neglected in (4.1).

The amplitude variance $\langle(\Delta\hat{A})^2\rangle$ is obtained by integrating (4.1) as

$$\langle(\Delta\hat{A})^2\rangle = \frac{1}{2\pi}\int_0^\infty P_{\Delta\hat{A}}(\Omega)d\Omega = \tfrac{1}{4} . \tag{4.6}$$

The amplitude variance is related to the photon number variance as

$$\begin{aligned}\langle(\Delta\hat{n})^2\rangle &= \langle[(A_0+\Delta\hat{A})^2 - A_0^2]^2\rangle \\ &= \langle[2A_0\,\Delta\hat{A} + (\Delta\hat{A})^2]^2\rangle \\ &\cong \langle(2A_0\,\Delta\hat{A})^2\rangle = 4\langle\hat{n}\rangle\langle(\Delta\hat{A})^2\rangle .\end{aligned} \tag{4.7}$$

Equation (4.6) is then rewritten in terms of the total photon number, $\hat{n}$, inside the cavity as $\langle(\Delta\hat{n})^2\rangle = \langle\hat{n}\rangle$.

In the same approximation as (4.3)—(4.5), the noise power spectrum of the internal field phase is given by (Appendix B)

$$P_{\Delta\hat{\phi}}(\Omega) = \frac{n_{sp}}{A_0^2\Omega^2}\frac{\omega}{Q}(1+\alpha^2) , \tag{4.8}$$

where $n_{sp} \equiv \langle\tilde{E}_{CV}\rangle/(\langle\tilde{E}_{CV}\rangle - \langle\tilde{E}_{VC}\rangle)$ is the so-called population inversion parameter. When $n_{sp}=1$ and $\alpha=0$, (4.8) reduces to

$$P_{\Delta\hat{\phi}}(\Omega) = \frac{1}{A_0^2\Omega^2}\frac{\omega}{Q} . \tag{4.9}$$

Figures 3 and 4 show these standard quantum limits for $P_{\Delta\hat{A}}(\Omega)(\omega/Q)$ and $2P_{\Delta\hat{\phi}}(\Omega)A_0^2\omega/Q$. The amplitude noise spectrum is Lorentzian, while the phase noise exhibits $\Omega^{-2}$ dependence, which reflects the nonstationary random-walk-type phase diffusion.

The oscillating field $\hat{a}$ inside the laser cavity couples out via the output mirror of the cavity. As shown in (3.2), the output wave $\hat{r}_1$ consists of the transmitted internal field $\hat{a}$ and the reflected zero-point fluctuation $\hat{f}$. Since $\hat{a}$ and $\hat{f}$ are quantum-mechanically correlated, as shown in (3.9), the quantum-mechanical interference between the two must be taken into account to calculate the $\hat{r}_1$ spectrum.

The output-wave fluctuation is expressed in terms of internal field fluctuation and the incident zero-point fluctuation as

$$\Delta\hat{r}_1 = \sqrt{\omega/Q_e}\,\Delta\hat{A} - \tfrac{1}{2}(\hat{f}e^{i\Delta\hat{\phi}} + e^{-i\Delta\hat{\phi}}\hat{f}^\dagger) \tag{4.10}$$

and

$$\Delta\hat{\psi}_1 = \Delta\hat{\phi} + \frac{1}{2ir_0}(\hat{f}e^{i\Delta\hat{\phi}} - e^{-i\Delta\hat{\phi}}\hat{f}^\dagger) , \tag{4.11}$$

where $\hat{r}_1$ is expressed by an equation similar to (3.16):

$$\hat{r}_1 = (r_0 + \Delta\hat{r}_1)e^{-i\Delta\hat{\psi}_1} . \tag{4.12}$$

The noise power spectrum for the output-wave amplitude is obtained (Appendix C) as

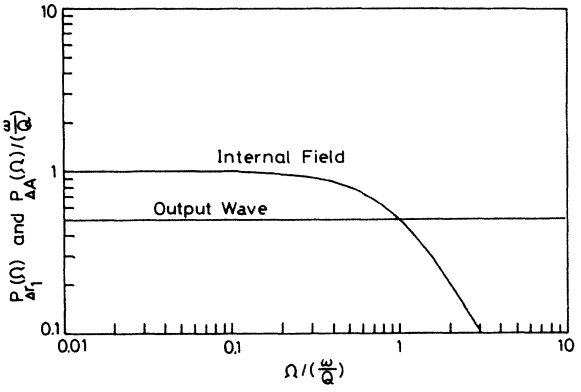


FIG. 3. Amplitude noise spectra of internal field $\hat{A}$ and output wave $\hat{r}_1$ for a free-running laser.

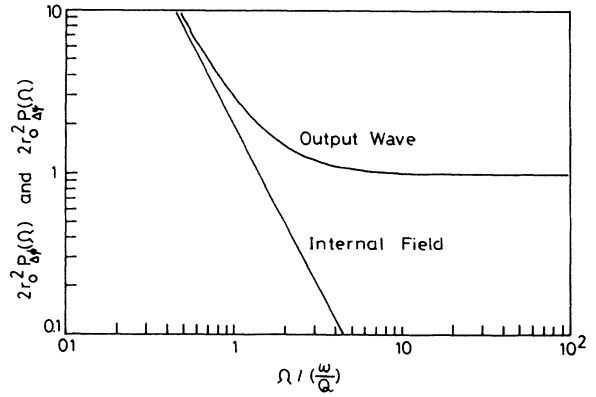


FIG. 4. Phase noise spectrum of the internal field $\hat{A}$ and the output wave $\hat{r}_1$ for a free-running laser.

$$P_{\Delta\hat{r}_1}(\Omega)=\left\{\frac{\omega}{Q_e}A_3^2P_{\tilde{F}_c}(\Omega)+\frac{\omega}{Q_e}(A_1^2+\Omega^2)P_{\hat{G}_r}(\Omega)+\left[\left[\frac{\omega}{Q_e}A_1-A_2A_3-\Omega^2\right]^2+\Omega^2\left[\frac{\omega}{Q_e}+A_1\right]^2\right]P_{\hat{f}_r}(\Omega)\right.$$
$$\left.-2A_1A_3\frac{\omega}{Q_e}\langle\tilde{F}_c(\Omega)\hat{G}_r(\Omega)\rangle\right\}\Big/[(A_2A_3+\Omega^2)^2+\Omega^2A_1^2]\ . \tag{4.13}$$

For a high pumping level, (4.13) is simplified as

$$P_{\Delta\hat{r}_1}(\Omega)=\tfrac{1}{2}\ . \tag{4.14}$$

Equation (4.14) can then be rewritten in terms of the single-sided power spectrum of the photon flux (number per second) $\hat{N}_1$ as

$$P_{\Delta\hat{N}_1}(\Omega)=4r_0^2P_{\Delta\hat{r}_1}(\Omega)=2\langle\hat{N}_1\rangle\ , \tag{4.15}$$

where $\langle\hat{N}\rangle$ is the average photon number per second. The amplitude noise power spectrum $P_{\Delta\hat{r}_1}(\Omega)$ for the output wave $\hat{r}_1$ is compared with $(\omega/Q)P_{\Delta\hat{A}}(\Omega)$ is Fig. 3. The power spectrum for the photon flux $\hat{N}_1$ is white and its spectral density $P_{\Delta\hat{N}_1}(\Omega)$ is equal to the familiar "shot noise" formula.

The noise power spectrum for the output-wave phase is similarly obtained as (Appendix C)

$$P_{\Delta\hat{\psi}_1}(\Omega)=\frac{\omega/Q}{A_0^2\Omega^2}+\frac{1}{2A_0^2\omega/Q_e}\ . \tag{4.16}$$

The first term comes from the nonstationary random-walk phase diffusion of the internal field, while the second term originates in the white noise due to the reflected zero-point fluctuation. The phase noise spectrum $2r_0^2P_{\Delta\hat{\psi}_1}(\Omega)$ for the output wave is compared with $2r_0^2P_{\Delta\hat{\phi}}(\Omega)$ in Fig. 4. Above the frequency region, $\Omega>\omega/Q$, the phase noise spectrum of the output wave is $1/2\langle N_1\rangle$.

For an arbitrary choice of a measurement time interval $T$ which is much shorter than $(\omega/Q)^{-1}$, the phase noise is given by integrating the second term of (4.16) over the Nyquist bandwidth $B=1/2T$ as

$$\langle(\Delta\psi_1)^2\rangle=\frac{1}{2A_0^2\omega/Q_e}\frac{1}{2T}=\frac{1}{4\langle\hat{n}_1\rangle}\ . \tag{4.17}$$

On the other hand, the photon number noise is calculated as

$$\langle(\Delta\hat{n}_1)^2\rangle=T^2\langle(\Delta\hat{N}_1)^2\rangle=T^2 2\langle\hat{N}_1\rangle/2T=\langle\hat{n}_1\rangle\ . \tag{4.18}$$

Equations (4.17) and (4.18) suggest that an ideal laser output can be regarded as a coherent state shown in Fig. 1(a). Under a free-running condition, an amplitude-squeezed state is not generated even though a bias level is much higher than the threshold and the laser is highly saturated.

The photon number noise (4.18) is actually the result of the subtle balance between the cooperative force (ordering force) and the entropy force (fluctuation). The cooperative force which stabilizes the amplitude stems from gain saturation, which can be enhanced by increasing a bias level. The entropy force which causes the amplitude fluctuation mainly stems from the pump fluctuation [the first term of the right hand side of (3.30)], and the field zero-point fluctuation [the first term of the right-hand side of (3.29)], when a bias level is well above the threshold. Unfortunately, these entropy forces are also enhanced with a bias level, resulting in the Poisson statistics for the photon number as (4.18). In the following sections, we will consider the possibility of introducing an artificial stabilization mechanism to break this balance favorably.

## V. QND MEASUREMENT OF A PHOTON-FLUX FLUCTUATION

In the proposed scheme, the photon-flux fluctuation $\Delta\hat{N}_1$ of the laser output wave is measured with a QND detector. The output current of the QND detector is negatively fed back to the semiconductor-laser pumping current. If the measurement error of the QND detector is zero, it can be shown that the output photon-flux noise is reduced arbitrarily by increasing the feedback gain. However, if there is a finite measurement uncertainty in the QND detector, the output noise cannot be decreased below a certain value. Furthermore, we are interested here in whether or not the generated photon state satisfies a minimum uncertainty product. In order to investigate these problems, it is essential to calculate the noise power spectra for the output-wave amplitude and phase, taking the QND measurement accuracy and its back action into account.

In this section, we will briefly describe the QND measurement of the photon-flux fluctuation via the optical Kerr effect.[21] A QND measurement via a four-wave mixing, which has the same interaction Hamiltonian as the optical Kerr effect, has been also proposed in Ref. 36. The present scheme uses the optical Kerr effect to measure the photon-flux fluctuation by the optical phase of a probe light.

The QND measurement scheme is shown in Fig. 5. The photon-flux operator of the laser output wave $\hat{r}_1$ is

$$\hat{N}_1=\hat{r}_1^{\dagger}\hat{r}_1\ . \tag{5.1}$$

The output wave whose photon-flux fluctuation is to be measured without being disturbed passes through the optical Kerr medium and the wavelength-selective mirrors $M_1$ and $M_2$, both of which are transparent at the wavelength of the laser output. The probe wave is coupled into the Kerr medium by $M_1$ and extracted by $M_2$. The reflectivities of the two mirrors are unity at the probe wavelength. The optical phase of the probe wave is shifted by the refractive-index change of the Kerr medium due to the laser output photon-flux fluctuation. The optical

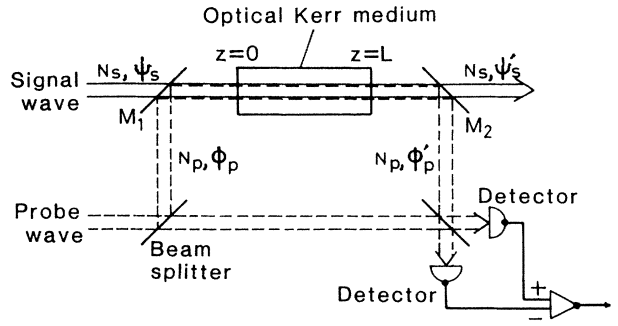


FIG. 5. Configuration of the QND detector for the photon number via the optical Kerr effect.

Kerr medium is assumed to have a transition level near $\omega+\omega_p$ as shown in Fig. 6. The third-order nonlinear process between the laser output wave and the probe wave is resonantly enhanced with the level, as is illustrated in Fig. 6(a), while four-photon processes within laser output wave and within probe wave are off resonant, which are, respectively, shown in Figs. 6(b) and 6(c). Therefore, the self-phase modulation effect for the laser output and probe wave is neglected. We also assume that $\omega+\omega_p$ is slightly detuned from the transition level so that the real absorption is negligible. In other words, an optical Kerr medium works in a dispersive-limit (reactive) region rather than in an absorptive-limit (resistive) region. The output current of the balanced-mixer homodyne detector "measures" the following operator (Appendix D):

$$\Delta\hat{N}_1^{\rm obs}=\Delta\hat{N}_1-\Delta\hat{\phi}_p(0)/(F')^{1/2}\ , \tag{5.2}$$

where $\Delta\hat{N}_1\equiv\Delta(\hat{r}_1^{\dagger}\hat{r}_1)$ is the photon flux of the laser output wave, $\hat{r}_1$, $\Delta\hat{\phi}_p(0)$ is the quantum noise of the probe wave without the Kerr medium, and $F'$, the constant which indicates the magnitude of the optical Kerr effect, is expressed as

$$(F')^{1/2}=\frac{\hbar\omega_p\omega\chi^{(3)}L}{2\epsilon_0\epsilon c^2A}\ . \tag{5.3}$$

Here, $\omega$ is the angular frequency for the laser output wave, $\omega_p$ the angular frequency for the probe wave, $\chi^{(3)}$ the third-order nonlinear susceptibility for the optical Kerr effect, $L$ the Kerr medium length, $\epsilon_0$ the dielectric constant for the vacuum space, $\epsilon$ the dielectric constant for the Kerr medium, $c$ the light velocity in the vacuum space, and $A$ is the cross-sectional area of the optical beam.

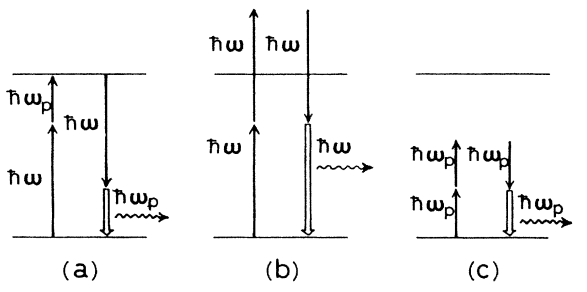


FIG. 6. Four-photon process for the optical Kerr effect: (a) mutual-phase-modulation effect (resonant with an actual level), (b) self-modulation effect for the signal wave (off resonant), (c) self-modulation effect for the probe wave (off resonant).

In (3.15), the quantum-mechanical pumping process is split into the rate term $p$ and the fluctuation term $\tilde{F}_c(t)$ by using the quantum-mechanical fluctuation-dissipation theorem.[22] That is to say, pumping rate $p$ is treated as a $c$-number. Since the deviation of the photon flux from the standard value, $\Delta\hat{N}_1^{\rm obs}=\hat{N}_1^{\rm obs}-\langle\hat{N}_1^{\rm obs}\rangle$, is fed back, the pumping current is now treated as an operator $\hat{p}$, which is expressed by the feedback gain $h$ as

$$\hat{p}(t)\equiv p-h\,\Delta\hat{N}_1^{\rm obs}=p-h[\Delta\hat{N}_1-\Delta\hat{\phi}_p(0)/(F')^{1/2}]$$

$$=p-2hr_0\,\Delta\hat{r}_1+h\,\Delta\hat{\phi}_p(0)/(F')^{1/2}\ , \tag{5.4}$$

This equation will be used for calculating the noise power spectra of the feedback laser. The last term, $h\,\Delta\hat{\phi}_p(0)/(F')^{1/2}$, means that the phase noise of the probe wave is added to the feedback signal and becomes the new Langevin noise source introduced by feedback. But its effect can be reduced by increasing the magnitude of the optical Kerr effect, $(F')^{1/2}$. In the next section, we calculate the noise power spectra of the laser output wave $\hat{r}_1$. Since the QND measurement does not affect the output-wave photon-flux fluctuation, this noise power spectrum also expresses that for the output wave $\hat{r}_2$, taken out of a feedback loop.

The optical phase $\hat{\psi}_2$ of the output wave $\hat{r}_2$ is similarly expressed as (Appendix D)

$$\hat{\psi}_2=\hat{\psi}_1-(F')^{1/2}\hat{N}_p\ , \tag{5.5}$$

where $\hat{\psi}_1$ is the phase of the output wave $\hat{r}_1$, and $\hat{N}_p$ is the photon flux of the probe wave. The second term of (5.5) represents the extra phase shift of the output wave due to the presence of the probe wave in the Kerr medium, which is also resonantly enhanced as is shown in Fig. 6. The photon flux noise $\Delta\hat{N}_p$ of the probe wave then adds extra phase noise $\Delta\hat{\psi}_2$ on the output wave $r_2$ as

$$\Delta\hat{\psi}_2=\Delta\hat{\psi}_1-(F')^{1/2}\Delta\hat{N}_p\ . \tag{5.6}$$

This is the back action of the QND measurement.

When an optical Kerr medium does not have a transition level near $\omega+\omega_p$, the self-phase-modulation effects should be taken into account as well as the above two mutual-phase-modulation effects (5.2) and (5.6) which are used for the QND measurement and responsible for the back action, respectively. Even in such a case, (5.2) holds if the probe-wave photon-flux fluctuation is much smaller than that of the signal wave. However, the back action (5.6) becomes large due to the self-phase-modulation of the signal wave. In the next section, we will see the minimum back action of (5.6) is necessary for satisfying a minimum uncertainty product for an amplitude-squeezed output wave $\hat{r}_2$. The assumption of a resonant enhanced Kerr effect is not essential, provided that only amplitude squeezing is concerned.

## VI. AMPLITUDE AND PHASE NOISE SPECTRA OF THE FEEDBACK LASER

This section deals chiefly with the purpose of the theoretical part of this paper. The amplitude and phase noise power spectra of the internal field and the output wave of the feedback laser are obtained. It will be shown here that the generated wave $\hat{r}_2$ is an amplitude-squeezed state in the sense that the amplitude noise power spectrum is reduced below the quantum noise level. It will also be demonstrated that the generated wave is in a minimum uncertainty state, that is, that the uncertainty product of the photon number and phase satisfies the equality sign of the Heisenberg's uncertainty relationship.

The working equations used here are as follows: the Langevin equations for the internal field amplitude, phase, and carrier, (3.24), (3.25), and (3.26); the relationship between the internal field and the output wave, (4.10) and (4.11); the pumping operator fed back after the QND measurement, (5.4); and the phase fluctuation imposed on the output wave $\hat{r}_2$ through the QND measurement, (5.6).

Using (3.26) and (5.4), the Langevin equation for the carrier number fluctuation $\tilde{N}_c$ is obtained as

$$\frac{d}{dt}\Delta\hat{N}_c=-h[2r_0\Delta\hat{r}_1+\Delta\hat{\phi}_p(0)/(F')^{1/2}]-\left[\frac{1}{\tau_{sp}}+\frac{1}{\tau_{st}}\right]\Delta\tilde{N}_c-\frac{2A_0}{\tau_{ph}}\Delta\hat{A}+\tilde{F}_c\ . \quad (6.1)$$

This equation is similar to (3.26) except for the feedback term (the first term in the right-hand side).

Fourier analysis of (3.24), (6.1), and (4.10) leads to the amplitude power spectrum for the output wave $\hat{r}_1$ (Appendix E) as

$$P_{\Delta\hat{r}_1}(\Omega)=\frac{1}{2}\left[\left[\frac{\omega}{Q_e}\right]^2+\Omega^2+\frac{h^2}{2F'r_0^2}\frac{\omega}{Q_e}P_{\Delta\hat{\phi}_p}(\Omega)\right]\Big/\left[\left[\frac{\omega}{Q_e}\right]^2(1+h)^2+\Omega^2\right], \quad (6.2)$$

where $P_{\Delta\hat{\phi}_p}(\Omega)$ is the phase noise spectrum of the probe wave. Here, a laser bias level is assumed well above the threshold. In the two limiting cases of $h\to 0$ and $h\to\infty$, (6.2) becomes

$$\lim_{h\to 0}P_{\Delta\hat{r}_1}(\Omega)=\tfrac{1}{2}\ , \quad (6.3)$$

and

$$\lim_{h\to\infty}P_{\Delta\hat{r}_1}(\Omega)=P_{\Delta\hat{\phi}_p}(\Omega)/4F'r_0^2\ . \quad (6.4)$$

Equation (6.3) coincides with the free running case, (4.14). Equation (6.4) means that the ultimate amplitude noise spectrum is determined by the phase noise spectrum of the probe wave divided by $4F'r_0^2$. The residual amplitude noise can thus be reduced by increasing the magnitude of the optical Kerr effect, $F'$. The amplitude noise spectra $P_{\Delta\hat{r}_2}(\Omega)=P_{\Delta\hat{r}_1}(\Omega)$ of an output wave for various values of feedback gain, $h$, are shown in Fig. 7.

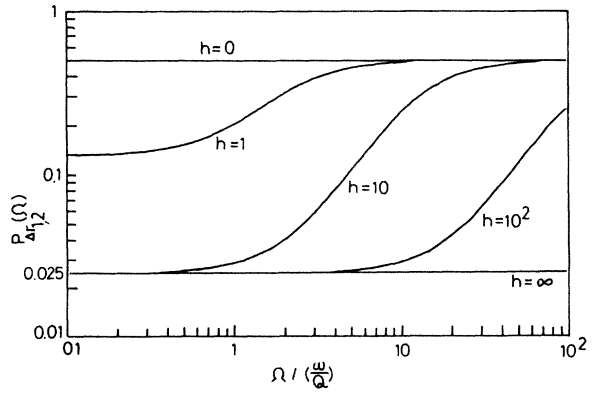


FIG. 7. Amplitude noise spectrum of the output wave $\hat{r}_2$ with QND measurement and feedback. $P_{\Delta\hat{\phi}_p}(\Omega)/4F'r_0^2$ in (6.4) is assumed to be 0.025, which is smaller than the noise level for a free-running laser by a factor of 20.

The phase noise spectrum for the output wave, $P_{\Delta\hat{\psi}_2}(\Omega)$, is similarly obtained using (3.24), (3.25), (6.1), and (4.11) as (Appendix E)

$$P_{\Delta\hat{\psi}_2}(\Omega)=\frac{(\omega/Q_e)^2}{r_0^2\Omega^2}+\frac{1}{2r_0^2}+F'P_{\Delta\hat{N}_p}(\Omega)\ . \quad (6.5)$$

The first term stems from the nonstationary random-walk phase diffusion of the internal field, and the second term is originated in the white noise due to the reflected zero-point fluctuation. The third term is caused by the photon flux noise of the probe wave, which is imposed on the output wave via the optical Kerr effect. The feedback gain $h$ does not affect the phase noise because $\alpha=0$ is assumed here. The phase noise spectrum $2r_0^2P_{\Delta\psi_2}(\Omega)$ of the output wave $\hat{r}_2$ with the QND measurement and feedback is shown in Fig. 8.

Next, let us consider the uncertainty relationship between the photon number and phase of the output wave $\hat{r}_2$. The first and second terms in (6.5) are negligible compared with the third term if we consider a large $F'$ value and higher $\Omega$ frequency region. The phase diffusion noise is dominant only in the low-frequency region and is usually suppressed by a phase-locked loop in a homodyne detector. Equation (6.5) then becomes

$$P_{\Delta\hat{\psi}_2}(\Omega)=F'P_{\Delta\hat{N}_p}(\Omega)\ . \quad (6.6)$$

Equation (6.4) is subsequently rewritten in terms of the noise spectrum of the photon flux as

$$P_{\Delta\hat{N}_2}(\Omega)=4r_0^2P_{\Delta\hat{r}_2}(\Omega)=P_{\Delta\hat{\phi}_p}(\Omega)/F'\ . \quad (6.7)$$

For an arbitrary choice of a measurement time interval $T$, the photon number uncertainty and phase uncertainty are given by integrating (6.6) and (6.7) over the Nyquist bandwidth $B=1/2T$ as

$$\langle(\Delta\hat{n}_2)^2\rangle=T^2\langle(\Delta\hat{N}_2)^2\rangle=(T^2/F')\langle(\Delta\hat{\phi}_p)^2\rangle\ , \quad (6.8)$$

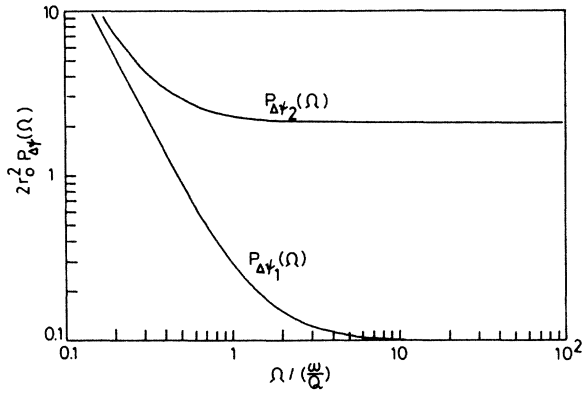


FIG. 8. Phase noise spectrum of the output wave $\hat{r}_2$ with QND measurement and feedback. $F'P_{\Delta\hat{N}_p}(\Omega)$ in (6.5) is assumed to be $10/r_0^2$, which is the minimum uncertainty noise under the assumption for Fig. 7. The phase noise is increased by a factor of 20 (in the region $\Omega > \omega/Q$).

and

$$\langle(\Delta\hat{\psi}_2)^2\rangle = F'\langle(\Delta\hat{N}_p)^2\rangle \ . \tag{6.9}$$

The product of (6.8) and (6.9) reduces to the uncertainty product of a probe wave as

$$\langle(\Delta\hat{n}_2)^2\rangle\langle(\Delta\hat{\psi}_2)\rangle = T^2\langle(\Delta\hat{N}_p)^2\rangle\langle(\Delta\hat{\phi}_p)^2\rangle = \langle(\Delta\hat{n}_p)^2\rangle\langle(\Delta\hat{\phi}_p)^2\rangle \ . \tag{6.10}$$

As is discussed in the Appendix of Ref. 21, the origins of the photon number noise $\langle(\Delta\hat{n}_p)^2\rangle$ and phase noise $\langle(\Delta\hat{\phi}_p)^2\rangle$ are, respectively, the quadrature noise components $\langle(\Delta\hat{b}_1)^2\rangle$ and $\langle(\Delta\hat{b}_2)^2\rangle$ of the zero-point fluctuation $\hat{b}$ incident upon beam splitter 1 from an unused port when the transmissivity of the beam splitter is close to unity. Then we have

$$\langle(\Delta\hat{n}_p)^2\rangle \cong 4\langle\hat{n}_p\rangle\langle(\Delta\hat{b}_1)^2\rangle = \langle\hat{n}_p\rangle \ , \tag{6.11}$$

$$\langle(\Delta\hat{\phi})^2\rangle \cong \langle(\Delta\hat{b}_2)^2\rangle/\langle\hat{n}_p\rangle = 1/4\langle\hat{n}_p\rangle \ . \tag{6.12}$$

Thus (6.10) equals $\frac{1}{4}$, which means that the output wave is in a number-phase minimum uncertainty state. Equations (6.8) and (6.9) indicate that the uncertainty of the photon number and phase can be controlled to an arbitrary value under the constraint of (6.10) by the factor $F'$. The output photon number noise can be reduced by increasing the length $L$ or $\chi^{(3)}$ of the optical Kerr medium at the cost of increased phase noise. This is referred to as an amplitude-squeezed state.

## VII. EXPERIMENTAL SETUP AND CALIBRATION OF QUANTUM NOISE LEVEL

In this as well as the subsequent section, we will describe the experimental result which verifies the first assumption in the theoretical analysis. This is that negative feedback does not introduce an additional noise source except the probe-wave phase noise in a QND detector, and, therefore, can suppress not only the excess noise but also the quantum noise. The experimental result also indicates that a conventional photon-flux measurement having a beam splitter followed by a photodetector cannot extract an amplitude-squeezed state outside of the feedback loop and that a QND measurement is an essential process for the proposed scheme.

The experimental setup is shown in Fig. 9(a). A single-frequency GaAs/AlGaAs semiconductor laser having a 0.82-$\mu$m oscillation wavelength was used at a bias level of $I/I_{\text{th}}=2$–3. The laser output photon-flux fluctuation was detected by a Si photodiode having a quantum efficiency larger than 0.8. The phase-reversed and amplified photocurrent fluctuation is superposed on a dc bias current to counteract the laser output photon-flux fluctuation.

The photocurrent fluctuation was connected to the noise spectrum measurement circuit and to the photoelectron statistics measurement circuit shown in Fig. 9(c). The photocurrent fluctuation spectrum was measured with a spectrum analyzer (HP 8568A). The photoelectron statistics were measured using the analog photon-counting technique[37] with the integrator (LPF; Anritsu MN51A), the sampling oscilloscope (Tektronix 7904-s2), and the digital wave memory (Kikusui 87025) having 50–64 channels. The data number for each photoelectron counting measurement is $3\times10^5$.

Another experimental setup is shown in Fig. 9(b). The laser output was equally divided by a 50%-50% beam splitter to illuminate two identical Si photodiodes having a quantum efficiency larger than 0.8. The five differential amplifiers were carefully chosen so as to keep the overall gains from the photodiodes to the three output terminals $A$, $B$, and $C$ exactly equal and flat over the measurement bandwidth up to 15 MHz. The photocurrent fluctuation at terminal $A$ was negatively fed back to the injection

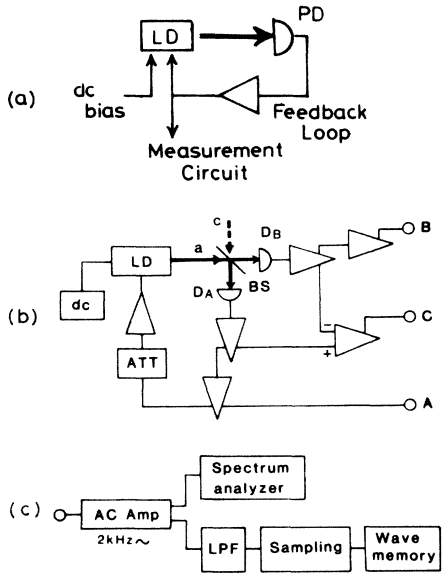


FIG. 9. Configuration of the experimental setup: (a) the negative-feedback semiconductor laser having a photodetector and (b) that having a balanced-mixer photodetector. (c) The photocurrent fluctuation spectrum and photoelectron statistics measurement circuits.

current of the laser diode in a way similar to that in Fig. 9(a).

In the next section we will describe the fact that the photocurrent fluctuation spectral density is lower than the quantum noise level, i.e., the shot noise level, and that the photoelectron statistics are narrower than the Poisson distribution. These experimental results cannot be explained without assuming that the laser output wave has the reduced photon-flux noise spectrum below the standard quantum limit and the sub-Poissonian photon statistics. We will also demonstrate that such a sub-Poissonian light cannot be extracted outside of a feedback loop by the configuration shown in Fig. 9(b). That is, the incident wave on photodiode $A$ has a photon-flux noise spectrum reduced below the quantum noise level and the sub-Poissonian photon statistics. On the other hand, the output wave to photodiode $B$ exhibits an enhanced photon-flux noise spectrum above the quantum noise level and super-Poissonian phonon statistics.

In order to confirm these experimental results, the quantum noise spectral density and the Poissonian photon statitics should be calibrated as the absolute level. Identifying the absolute quantum noise levels in experiments is difficult, because the Si photodiode quantum efficiency is not constant. Rather it indicates a dependence on the fluctuation frequency. It is additionally difficult because the absolute power level displayed on the spectrum analyzer is not reliable. Furthermore, identifying the Poissonian photon statistics is complex because a conventional digital photon counter having a threshold decision is incapable of handling a large number of photoelectrons on the order of $10^8$, as in the present case.

In order to overcome such difficulties, the measurement circuits shown in Fig. 9(c) were calibrated by an incoherent GaAs light-emitting-diode (LED) output. The measurement time interval $T \cong 10^{-7}$–$10^{-8}$ sec in our experiment is much longer than a coherence time $\tau_c$, which is on the order of $10^{-12}$ sec for a GaAs LED. The LED light therefore produces the quantum noise spectrum and the Poissonian photon statistics.[38]

The measured intensity noise spectrum is compared with the quantum noise level $2eI_p$ in Fig. 10, where $I_p$ is a photocurrent. The photocurrent noise power spectrum $P_{\text{in}}(\Omega)$ measured with the spectrum analyzer is transformed into the primary current noise spectrum by $P_{\text{in}}(\Omega)/GB$, where $G$ is the measured electronic amplifier circuit power gain and $B$ is the separately calibrated resolution bandwidth of the spectrum analyzer. It is further transformed into the excess noise factor $\chi_1$, defined as the photocurrent spectral density divided by the quantum noise level as

$$\chi_1 = P_{\text{in}}(\Omega)/2eI_pGB \ . \tag{7.1}$$

The thermal noise added by the electronic amplifier was removed by a light chopper and the phase-sensitive detection using a lock-in amplifier. The experimental result deviates from the theoretical value only by less than 0.05 dB in the frequency region from dc to 15 MHz. This can be considered as the accuracy of the present photon flux noise spectrum measurement.

The measured and calculated photon statistics are compared in Fig. 11. The integrated photocurrent $\Lambda = \int_t^{t+T} i(t)dt$ over the measurement time interval $T$ is transformed into the primary photoelectron number $n$ by the relation $n = \Lambda/e\sqrt{G}$. The theoretical Poissonian distribution is calculated by $P(n) = e^{-\langle n \rangle}\langle n \rangle^n/n!$, where $\langle n \rangle$ is the average number of primary photoelectrons and is given by $\langle n \rangle = I_pT/e$. The agreement between the experimental and theoretical Poissonian statistics is fairly good. The slight deviation is due to thermal noise contribution, which cannot be excluded in the analog photoelectron counting. However, it is possible to eliminate

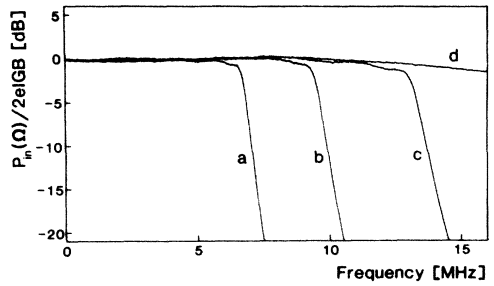


FIG. 10. Normalized photocurrent fluctuation spectrum, $P_{\text{in}}(\Omega)/2eI_pGB$, for a GaAs LED output. Curves $a$–$d$ correspond to the use of low-pass filters with bandwidths of 6.713, 9.463, 13.10 MHz, and without a filter, respectively.

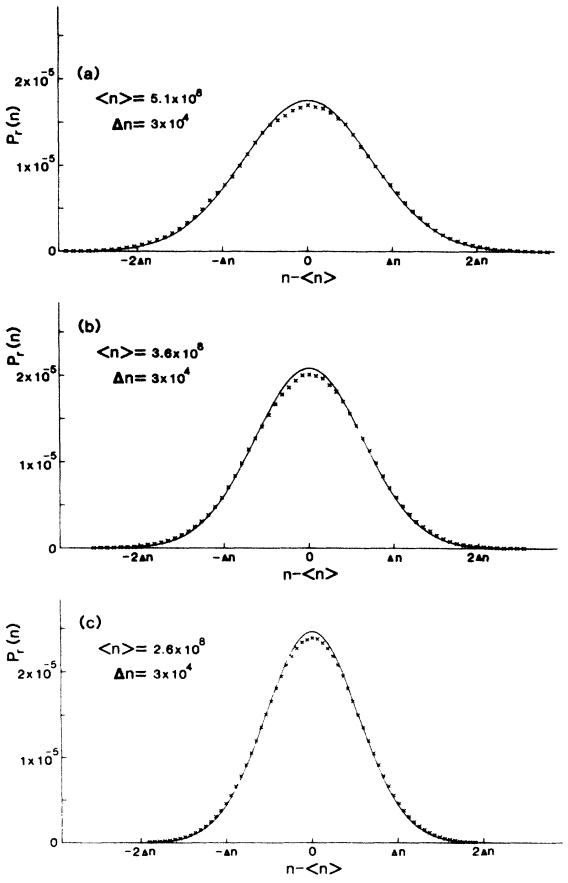


FIG. 11. The photoelectron statistics $P_r(n)$ for a GaAs LED output. The counting time intervals are (a) 38, (b) 53, and (c) 74 ns. Solid lines are the theoretical Poisson distributions.

the effect of the thermal noise from the evaluation of the excess noise factor $\chi_2$. If the normalized second moment $X$ of a photoelectron number is defined as

$$X \equiv [\langle (\Delta n)^2 \rangle - \langle n \rangle] / \langle n \rangle , \tag{7.2}$$

$X$ is related to the excess intensity noise factor $\chi_2$ as

$$\chi_2 - 1 = X . \tag{7.3}$$

We measured a zero mean thermal noise electron distribution by blocking the incident LED light and obtained the second moment of the thermal noise electron, $\langle (\Delta n)^2 \rangle_{\text{th}}$. The primary photoelectron second moment $\langle (\Delta n)^2 \rangle$ is obtained by the relation

$$\langle (\Delta n)^2 \rangle = \sum n^2 P(n) - \left[ \sum nP(n) \right]^2 - \langle (\Delta n)^2 \rangle_{\text{th}} . \tag{7.4}$$

When the photoelectron statistics $P(n)$ is Poissonian, the value of $X$ is zero, which corresponds to $\chi_2 = 1$. Table I summarizes the various values of $\chi_1$ obtained directly from the photocurrent spectral measurement and $\chi_2$ from the photoelectron counting measurement, using (7.1) and (7.3), respectively. As can be seen, the experimental results are very close to the theoretical value of $\chi = 1.0$.

## VIII. EXPERIMENTAL RESULTS

The photocurrent fluctuation spectra for the free-running and feedback-stabilized GaAs laser output [Fig. 9(a)] are shown in Fig. 12 with the calibrated quantum noise level produced by an LED light. While the photocurrent fluctuation spectrum for the free-running condition is higher than the quantum noise level by 4—5 dB, that for the feedback stabilization is reduced below this noise level by 6—7 dB, depending on the frequency. The photoelectron statistics for the free-running and feedback-stabilized GaAs laser output [Fig. 9(a)] are compared in Fig. 13 with the theoretical Poisson distribution.

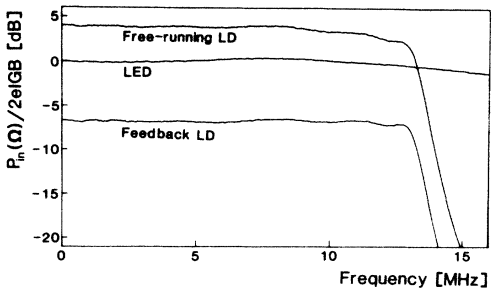


FIG. 12. Normalized photocurrent fluctuation spectral densities for free-running and negative-feedback semiconductor lasers having a single photodetector.

While the photoelectron statistics for the free-running condition are super-Poissonian, the sub-Poissonian statistics are obtained during the feedback stabilization.

The excess noise factors $\chi_1$ obtained from the photocurrent fluctuation spectrum and $\chi_2$ obtained from the photoelectron statistics are shown in Table I for the free-running and feedback-stabilization conditions. It is obvious that the observed sub-Poissonian photoelectron statistics and subquantum limit photocurrent fluctuation spectrum are much more dominant phenomena as opposed to the measurement uncertainty calibrated by using a LED light. Since the photoelectron emission process is a one-to-one correspondence with the photon arrival rate when the detector quantum efficiency is high, the above experimental results cannot be explained without assuming that the GaAs laser output features the sub-Poissonian photon statistics.

The photocurrent fluctuation spectra measured at terminals $A$ and $B$ for the free-running GaAs/AlGaAs semiconductor laser [Fig. 9(b)] are shown by the circles and plusses in Fig. 14 and compared with the theoretical quantum noise level shown by a solid line. The incident

TABLE I. The excess intensity noise factors $\chi_1$, obtained from the photocurrent fluctuation spectrum measurement (7.1), and $\chi_2$, obtained from the photoelectron counting measurement (7.3), for the three quantum noise level calibration cases using an LED light, a free-running semiconductor laser, and a feedback-stabilized semiconductor laser.

| Case | Detector bandwidth (measurement time interval) | $I_p$ (mA) | $\chi_1$ (Photocurrent fluctuation spectrum) | $\langle n \rangle$ | $\chi_2$ (Photoelectron counting) |
|---|---|---|---|---|---|
| Calibration with a LED | 6.713 MHz (74.48 nsec) | 1.10 | 1.005 (0.02 dB) | $5.114 \times 10^8$ | 1.0002 (0.001 dB) |
| | 9.463 MHz (52.84 nsec) | 1.10 | 0.9954 (−0.02 dB) | $3.628 \times 10^8$ | 1.003 (0.013 dB) |
| | 13.10 MHz (38.17 nsec) | 1.10 | 0.9908 (−0.04 dB) | $2.621 \times 10^8$ | 1.002 (0.008 dB) |
| Free-running GaAs laser | 13.10 MHz (38.17 nsec) | 1.10 | 2.747 (4.388 dB) | $2.621 \times 10^8$ | 2.821 (4.504 dB) |
| Feedback-stabilized GaAs laser | 13.10 MHz (38.17 nsec) | 1.10 | 0.207 (−6.848 dB) | $2.621 \times 10^8$ | 0.258 (−5.887 dB) |

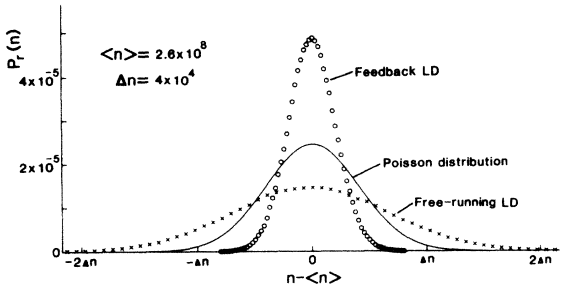


FIG. 13. Photoelectron statistics for free-running and negative-feedback semiconductor lasers with a single photodetector.

waves on the two Si photodiodes exhibit smaller excess noise than the result of the single detector shown in Fig. 12. This is because the semiconductor laser is biased higher and also because there optical loss is present between the laser and the photodiode, which contributes to the elimination of the excess noise of the incident wave.

When the feedback circuit was closed, the photocurrent noise spectra measured at terminals $A$ and $B$ become different as shown in Fig. 14. The noise spectrum at terminal $A$ was reduced by 5—10 dB below the quantum noise level. The difference is again much larger than the uncertainty of less than 0.05 dB in identifying the quantum noise level. This means that the incident wave on photodiode $A$ has its reduced photon-flux noise below the standard quantum limit. On the other hand, the noise spectrum at terminal $B$ was increased by about 3 dB above the quantum noise level. This means that the incident wave on photodiode $B$ has its photon-flux noise increased to twice that of the quantum noise level.

The photoelectron counting measurement exhibits the same behavior. The photoelectron statistics measured at terminal $A$ for free-running and feedback-stabilized cases are shown by the crosses and open circles in Fig. 15. The theoretical Poissonian distribution is shown by a solid line. It is clear in Fig. 15 that the super-Poissonian photoelectron statistics of a free-running laser output become sub-Poissonian through feedback stabilization. The experimental photoelectron statistics give the normalized

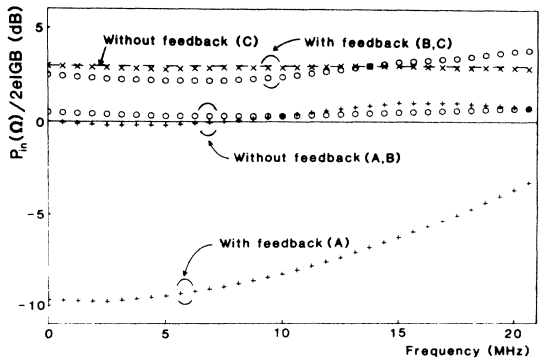


FIG. 14. Normalized photocurrent fluctuation spectral density for free-running and negative-feedback semiconductor lasers having a balanced-mixer photodetector. Solid line (0 dB) is the quantum noise level.

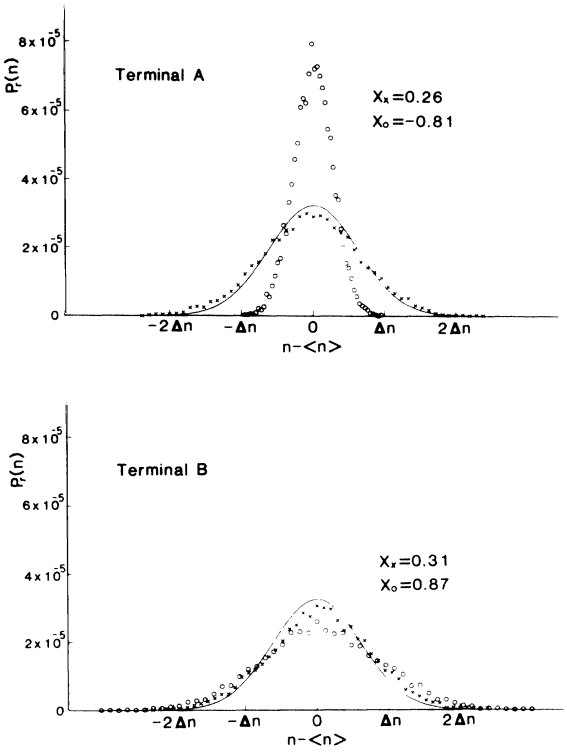


FIG. 15. Photoelectron statistics measured at terminals $A$ and $B$ for free-running and negative-feedback semiconductor lasers having a balanced-mixer photodetector. Solid lines are theoretical Poisson distributions; $\langle n\rangle = 1.5\times10^8$ and $\Delta n = 2\times10^4$.

second moment $X=-0.81$ in a feedback-stabilization case, which corresponds to the excess noise factor $\chi=0.19$ ($-7$ dB). This value is in fairly good agreement with the reduced photocurrent noise spectrum shown in Fig. 14. The photon statistics measured at terminal $B$, on the other hand, exhibit a super-Poissonian distribution for feedback stabilization which is broader than that for the free-running case. Again the measured value of $X=+0.87$ (or $\chi=1.87$) is in fairly good agreement with the enhanced photocurrent noise spectrum shown in Fig. 14.

These experimental results can be understood as follow: If the output wave from the semiconductor laser and the zero-point fluctuation incident on a beam splitter from an open port are designated by $\hat{r}_1$ and $\hat{c}$, the incidental waves on photodiodes $A$ and $B$ are given by

$$\hat{r}_A=(\hat{r}_1+\hat{c})/\sqrt{2}\ , \tag{8.1}$$

and

$$\hat{r}_B=(\hat{r}_1-\hat{c})/\sqrt{2}\ . \tag{8.2}$$

Here, $\hat{r}_1=(r_0+\Delta\hat{r}_1)e^{-i\Delta\hat{\psi}}$ and the zero-point fluctuation $\hat{c}\ (\equiv\hat{c}_1+i\hat{c}_2)$ satisfies

$$\langle\hat{c}_1\rangle=\langle\hat{c}_2\rangle=0\ . \tag{8.3}$$

If the photodiode quantum efficiency is unity, a dc photocurrent $i_{A0}$ is given by

$$i_{A0} \equiv e\langle \hat{r}_A^{\dagger} \hat{r}_A \rangle = er_0^2/2 \ . \tag{8.4}$$

The photocurrent fluctuation $\Delta i_A$ of photodiode $A$ measures the photon-flux fluctuation operator[8] as

$$\Delta \hat{i}_A \equiv 2e\langle \hat{r}_{A1} \rangle \Delta \hat{r}_{A1} = er_0(\Delta \hat{r}_1 + \hat{c}_1) \ . \tag{8.5}$$

The in-phase noise component $\hat{c}_1$ corresponds to the normalized phase noise of the probe wave in the previous QND measurement scheme. If (8.5) is used in the operator Langevin equation for a negative-feedback semiconductor laser instead of (5.2) for the QND scheme, the quantum-mechanical correlation is established by feedback stabilization as in

$$\Delta \hat{r}_1 = -\hat{c}_1 \quad (\text{for } h \to \infty) \ . \tag{8.6}$$

Consequently, the photon-flux fluctuation spectrum of the incident wave $\hat{r}_A$ on photodiode $A$ is reduced.

On the other hand, the intensity fluctuation spectrum of the output wave $\hat{r}_B$ in photodiode $B$ is

$$P_{\Delta \hat{r}_B}(\Omega) = 2P_{\Delta \hat{r}_1}(\Omega) \ . \tag{8.7}$$

Equation (8.7) explains the enhanced intensity noise spectral density and super-Poissonian photon statistics.

In order to confirm the above discussion, the photocurrent fluctuation spectral density and photoelectron statistics were measured at terminal $C$, that is, the subtracted output. The dc photocurrent at terminal $C$ is expressed as

$$i_{c0} \equiv e(\langle \hat{r}_A^{\dagger} \hat{r}_A \rangle - \langle \hat{r}_B^{\dagger} \hat{r}_B \rangle) = e(r_0^2 - r_0^2) = 0 \ . \tag{8.8}$$

The photocurrent fluctuation $\Delta i_c$ measures the following operator[39] as

$$\Delta \hat{i}_c \equiv 2e(\langle \hat{r}_{A1} \rangle \Delta r_{A1} - \langle \hat{r}_{B1} \rangle \Delta \hat{r}_{B1}) = 2er_0 \hat{c}_1 \ . \tag{8.9}$$

Equation (8.9) suggests that the photocurrent fluctuation $\Delta i_c$ measured at terminal $C$ reflects the beat noise between the coherent excitation of the laser output wave $r_0$ and the in-phase component of the zero-point fluctuation, $\hat{c}_1$. It further suggests that it is always standard quantum limited irrespective of the feedback stabilization. The photocurrent fluctuation spectral density measured at terminal $C$ for free-running and feedback-stabilization cases are shown by the crosses and triangles in Fig. 14. As indicated by (8.9), the spectral density is just 3 dB above the quantum noise level for terminals $A$ and $B$.

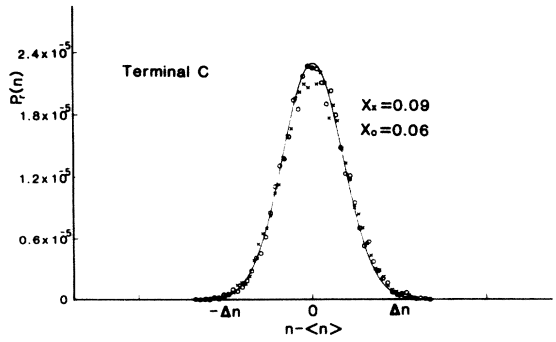


FIG. 16. Photoelectron statistics measured at terminal $C$ for free-running (○) and negative-feedback (×) semiconductor lasers having a balanced-mixer photodetector. Solid line is the theoretical Poissonian distribution; $\langle n \rangle = 3 \times 10^8$ and $\Delta n = 5 \times 10^4$.

The photoelectron counting statistics measured at terminal $C$ are shown in Fig. 16 for free-running and feedback-stabilization cases. Although the average photoelectron number was zero at terminal $C$, it was translated into the total photoelectron number $(i_{A0} + i_{B0})T/e$ in Fig. 16. These experimental results are in good agreement with the theoretical Poissonian distribution shown by a solid line.

## IX. DISCUSSION

The negative feedback is capable of suppressing the quantum noise of a laser output wave. Such nonclassical light, however, cannot be extracted outside of a feedback loop if a conventional (destructive) photon-flux measurement scheme is employed. In this respect, quantum nondemolition measurement plays an essential role in generating an amplitude-squeezed state. In fact, the enhanced phase noise, which compensates for the reduced photon number noise and defends Heisenberg's uncertainty principle $\langle (\Delta \hat{n})^2 \rangle \langle (\Delta \hat{\phi})^2 \rangle \geqq \frac{1}{4}$, is imposed in the QND process as a back action of the measurement. The commutator bracket for the output wave $\hat{r}_2$ is preserved properly under feedback stabilization due to the balance between the finite measurement uncertainty (5.2) and the finite back action on the conjugate observable (5.6). This point is extensively discussed in Ref. 20.

The scheme proposed in this paper is essentially different from the squeezed-state-generating schemes which utilize a unitary evolution in a variety of nonlinear optical processes. The most important feature of the proposed scheme is its capability to prepare (synthesize) any number-phase minimum uncertainty state in terms of the average photon number and the variance distribution between the photon number and phase. The average photon number can be assigned by a dc bias current, and the variance distribution can be determined by the magnitude of the Kerr effect, $F'$. When the QND measurement error goes to zero (i.e., $F' \to \infty$), the output wave approaches a "photon number eigenstate."

This is essentially different from the generation of a photon number eigenstate via wave function reduction only by a QND measurement.[40,41] If the photon system is conservative and the QND measurement of a photon number is ideal, the photon field falls into a photon number eigenstate after the measurement. However, no one can predict or control the eigenvalue for the resulting photon number eigenstate before the measurement. In this sense, the process is completely passive. Moreover, a laser oscillator is not a conservative system but a dissipative system. The output photon flux is subject to fluctuations and experiences time evolution due to the coupling with the reservoirs. Therefore, different eigenvalues are expected to result from one sample to next. The combination of QND measurement and negative feedback can overcome these two problems and can synthesize a desired quantum state.

## ACKNOWLEDGMENTS

The authors wish to thank Professor Hermann A. Haus of Massachusetts Institute of Technology for his useful discussions. They are also indebted to Fumio Kanaya of Musashino Electrical Communication Laboratories for his continuous encouragement.

## APPENDIX A

This appendix derives the quasilinearized Langevin equations (3.24)—(3.26) from the Langevin equations (3.9) and (3.15).

Substituting (3.16) into (3.9) and its Hermitian conjugate, we obtain

$$\frac{d}{dt}\Delta\hat{A}=-\frac{1}{2}\left[\frac{\omega}{Q_e}+\frac{\omega}{Q_0}-\frac{\omega}{\mu^2}\tilde{\chi}_i\right](A_0+\Delta\hat{A})+\hat{H}_r(t) \tag{A1}$$

and

$$\frac{d}{dt}\Delta\hat{\phi}=\frac{1}{2A_0}\frac{\omega}{\mu^2}\tilde{\chi}_r(A_0+\Delta\hat{A})+\frac{1}{A_0}\hat{H}_i(t)\ , \tag{A2}$$

where $\hat{H}_r(t)$ and $\hat{H}_i(t)$ are defined as in (3.27) and (3.28). Using (3.17)—(3.20) and neglecting the products of the fluctuation operators, (A1), (A2), and (3.15) become

$$\frac{d}{dt}\Delta\hat{A}=-\frac{1}{2}\left[\frac{\omega}{Q_e}+\frac{\omega}{Q_0}-\frac{\omega}{\mu^2}\langle\tilde{\chi}_i\rangle\right](A_0+\Delta\hat{A})+\frac{\omega}{2\mu^2}A_0\frac{d\langle\tilde{\chi}_i\rangle}{dN_{c0}}\Delta\tilde{N}_c+\hat{H}_r(t)\ , \tag{A3}$$

$$\frac{d}{dt}\Delta\hat{\phi}=\frac{\omega}{2A_0\mu^2}\langle\tilde{\chi}_r\rangle(A_0+\Delta\hat{A})+\frac{\omega}{2\mu^2}\frac{d\langle\tilde{\chi}_r\rangle}{dN_{c0}}\Delta\tilde{N}_c+\frac{1}{A_0}\hat{H}_i(t)\ , \tag{A4}$$

and

$$\frac{d}{dt}\Delta\tilde{N}_c=p-\frac{N_{c0}}{\tau_{sp}}-\frac{\omega}{\mu^2}\langle\tilde{\chi}_i\rangle A_0^2-\langle\tilde{E}_{CV}\rangle-\frac{\Delta\tilde{N}_c}{\tau_{sp}}-\frac{2\omega}{\mu^2}A_0^2\frac{d\langle\tilde{\chi}_i\rangle}{dN_{c0}}\Delta\tilde{N}_c-\frac{2\omega}{\mu^2}\langle\tilde{\chi}_i\rangle A_0\Delta\hat{A}+\tilde{F}_c(t)\ . \tag{A5}$$

The expectation values of (A3)—(A5) give the following relations:

$$\frac{\omega}{Q_e}+\frac{\omega}{Q_0}=\frac{1}{\tau_{ph}}=\langle\tilde{E}_{CV}\rangle-\langle\tilde{E}_{VC}\rangle\ , \tag{A6}$$

$$\omega=\omega_0-\frac{\omega}{\mu^2}\langle\tilde{\chi}_r\rangle\ , \tag{A7}$$

and

$$p=\frac{N_{c0}}{\tau_{sp}}+A_0^2(\langle\tilde{E}_{CV}\rangle-\langle\tilde{E}_{VC}\rangle)-\langle\tilde{E}_{CV}\rangle\ , \tag{A8}$$

where (3.12) is used. Using the relations (A6)—(A8) and notations (3.21)—(3.23) and (3.12), (A3)—(A5) are rewritten as (3.24)—(3.26).

## APPENDIX B

In this appendix the amplitude and phase noise spectra are obtained for the *internal* field with no feedback. Equations (4.1) and (4.9) are derived from the Langevin equations (3.24)—(3.26) and the correlation functions (3.29)—(3.32).

First we delineate the definition and the calculation procedure for a single-sided power spectral density per unit cps. The power spectrum $P_{\hat{q}}(\Omega)$ of an operator $\hat{q}(t)$ which is a nonperiodically fluctuating function of $t$ is given by

$$P_{\hat{q}}(\Omega)\equiv 2\int_{-\infty}^{\infty}\langle\hat{q}^{\dagger}(t+\tau)\hat{q}(t)\rangle e^{-i\Omega\tau}d\tau\ . \tag{B1}$$

Parseval's theorem gives the normalization of the single-sided power spectrum as

$$\int_0^{\infty}P_{\hat{q}}(\Omega)\frac{d\Omega}{2\pi}=\langle\hat{q}^{\dagger}(t)\hat{q}(t)\rangle\ . \tag{B2}$$

Definition (B1) is used to obtain the power spectrum from correlation functions.

Another formula for $P_{\hat{q}}(\Omega)$ is given by Wiener-Khintchin's theorem as

$$P_{\hat{q}}(\Omega)=\lim_{T\to\infty}\langle\hat{Q}^{\dagger}(T,\Omega)\hat{Q}(T,\Omega)\rangle\ , \tag{B3}$$

where $\hat{Q}(T,\Omega)$ is the finite Fourier transform of $\hat{q}(t)$ defined as

$$\hat{Q}(T,\Omega)\equiv\sqrt{2/T}\int_{-T/2}^{T/2}\hat{q}(t)e^{-i\Omega t}dt\ . \tag{B4}$$

Definition (B3) is used to calculate the power spectrum from the Langevin equations.

The finite Fourier transform of $d\hat{q}(t)/dt$ is obtained, using integration by parts, as

$$\hat{Q}_1(T,\Omega)\equiv\sqrt{2/T}\,[\hat{q}(T/2)e^{-i\Omega T/2}-\hat{q}(-T/2)e^{i\Omega T/2}]+i\Omega\hat{Q}(T,\Omega)\ . \tag{B5}$$

Since the first term vanishes within the limit of $T\to\infty$, the finite Fourier transform can be treated as a usual Fourier transform in the sense that time derivative is expressed by multiplying $i\Omega$ in the $\Omega$ space. This is used in the calculation of the finite Fourier transform of the Langevin equations. We omit $T$ hereafter since it plays no role in the calculation. Furthermore, the term "Fourier transform" will be used instead of "finite Fourier transform" for the sake of simplicity.

The Fourier transforms of (3.24)—(3.26) are then expressed as

$$i\Omega\Delta\hat{A}(\Omega)=A_3\Delta\tilde{N}_c(\Omega)+\hat{H}_r(\Omega)\ , \tag{B6}$$

$$i\Omega\Delta\hat{\phi}(\Omega)=A_4\Delta\tilde{N}_c(\Omega)+\hat{H}_i(\Omega)/A_0\ , \tag{B7}$$

and

$$i\Omega\Delta\tilde{N}_c(\Omega)=A_1\Delta\tilde{N}_c(\Omega)+A_2\Delta\hat{A}(\Omega)+\tilde{F}_c(\Omega)\ , \tag{B8}$$

where

$$A_1=-(1/\tau_{sp})-(1/\tau_{st}) , \tag{B9}$$

$$A_2=-2A_0/\tau_{ph} , \tag{B10}$$

$$A_3=1/2A_0\tau_{st} , \tag{B11}$$

and

$$A_4=\alpha/2A_0^2\tau_{st} . \tag{B12}$$

Eliminating $\Delta\tilde{N}_c$ from (B6) and (B8), we obtain

$$\Delta\hat{A}(\Omega)=[-A_3\tilde{F}_c+(A_1-i\Omega)\hat{H}_r]/(A_2A_3+\Omega^2+i\Omega A_1) . \tag{B13}$$

Using (B3), the power spectrum $P_{\Delta\hat{A}}(\Omega)$ is obtained as

$$P_{\Delta\hat{A}}(\Omega)=\frac{A_3^2P_{\tilde{F}c}(\Omega)+(\Omega^2+A_1^2)P_{\hat{H}r}(\Omega)-2A_1A_3\langle\hat{H}_r(\Omega)\tilde{F}_c(\Omega)\rangle}{(\Omega^2+A_2A_3)^2+\Omega^2A_1^2}$$

$$=\frac{(A_3^2/A_1^2)P_{\tilde{F}c}(\Omega)+(1+\Omega^2/A_1^2)P_{\hat{H}r}(\Omega)-2(A_3/A_1)\langle\hat{H}_r(\Omega)\tilde{F}_c(\Omega)\rangle}{(A_2A_3/A_1)^2+\Omega^2(1+\Omega^2/A_1^2+2A_2A_3/A_1^2)} . \tag{B14}$$

When a laser is biased at well above the lasing threshold, $1/\tau_{st}$ can be much larger than all the other lifetime constants such as $1/\tau_{ph}$ and $1/\tau_{sp}$. For such a bias level, we need to consider only the fluctuation frequency below $1/\tau_{st}$ and then can use the approximation

$$\Omega\ll|A_1| , \tag{B15}$$

$$A_3/A_1=\frac{-1}{2A_0\tau_{st}}\left[\frac{1}{\tau_{sp}}+\frac{1}{\tau_{st}}\right]^{-1}\cong\frac{-1}{2A_0} , \tag{B16}$$

$$A_2A_3/A_1\cong 1/\tau_{ph} , \tag{B17}$$

and

$$A_2A_3/A_1^2\ll 1 . \tag{B18}$$

Using these relations, (B14) is rewritten as

$$P_{\Delta\hat{A}}(\Omega)=\frac{P_{\tilde{F}c}(\Omega)/4A_0^2+P_{\hat{H}r}(\Omega)+\frac{1}{A_0}\langle\hat{H}_r(\Omega)\tilde{F}_c(\Omega)\rangle}{(\Omega^2+1/\tau_{ph}^2)} . \tag{B19}$$

The power spectra $P_{\tilde{F}c}(\Omega)$, $P_{\hat{H}r}(\Omega)$, and $\langle\hat{H}_r(\Omega)\tilde{F}_c(\Omega)\rangle$ are obtained from the correlation functions (3.29)—(3.32) using (B1). The power spectrum $P_{\Delta\hat{A}}(\Omega)$ is then rewritten as

$$P_{\Delta\hat{A}}(\Omega)=[(n_{th}+1)/\tau_{ph}+N_{c0}/\tau_{sp}A_0^2]/(\Omega^2+1/\tau_{ph}^2) , \tag{B20}$$

where relations (A8) and (A10) are used. For a high pumping, the term $N_{c0}/\tau_{sp}A_0^2$ in (B20) is negligible compared with the term $(n_{th}+1)/\tau_{ph}$. Equation (B20) is then rewritten as (4.1), where $n_{th}$ is neglected as a small quantity.

The phase noise spectrum is obtained in a similar way. Eliminating $\Delta\hat{A}$ and $\Delta\tilde{N}_c$ from (B6)—(B8), we obtain

$$\Delta\hat{\phi}(\Omega)=[iA_2A_4\hat{H}_r(\Omega)/\Omega-A_4\tilde{F}_c]/(A_2A_3+\Omega^2+i\Omega A_1)$$

$$+\hat{H}_i(\Omega)/\Omega A_0 . \tag{B21}$$

This leads to the phase noise spectrum

$$P_{\Delta\hat{\phi}}(\Omega)=[(A_2A_4/\Omega)^2P_{\hat{H}r}(\Omega)$$

$$+A_4^2P_{\tilde{F}c}(\Omega)]/[(A_2A_3+\Omega^2)^2+\Omega^2A_1^2]$$

$$+P_{\hat{H}i}(\Omega)/\Omega^2A_0^2 . \tag{B22}$$

Using the same approximations mentioned above and relations

$$A_4/A_1\cong-\alpha/2A_0^2 , \tag{B23}$$

$$A_2A_4/A_1\Omega\cong\alpha/A_0\tau_{ph}\Omega , \tag{B24}$$

and (3.29)—(3.32), Eq. (B22) is rewritten as

$$P_{\Delta\hat{\phi}}(\Omega)=[(1+\alpha^2)n_{sp}]/A_0^2\tau_{ph}\Omega^2 , \tag{B25}$$

where $n_{sp}\equiv\langle\tilde{E}_{CV}\rangle/(\langle\tilde{E}_{CV}\rangle-\langle\tilde{E}_{VC}\rangle)$ is the population inversion parameter. Equation (B25) is identical to (4.8).

## APPENDIX C

This appendix describes the calculation procedure of the amplitude and phase noise spectra for the *output* wave $\hat{r}_1$ with no feedback. Equations (4.13) and (4.16) are derived from (4.10) and (4.11).

The Fourier transforms (Appendix B) of (4.10) and (4.11) are expressed as

$$\Delta\hat{r}_1(\Omega)=\sqrt{\omega/Q_e}\,\Delta\hat{A}(\Omega)-\hat{f}_r(\Omega) , \tag{C1}$$

and

$$\Delta\hat{\psi}(\Omega)=\Delta\hat{\phi}(\Omega)+\hat{f}_i(\Omega)/r_0 , \tag{C2}$$

where $\hat{f}_r(\Omega)$ is the Fourier transform of

$$\hat{f}_r(t)\equiv[\hat{f}(t)e^{i\Delta\hat{\phi}(t)}+e^{-i\Delta\hat{\phi}(t)}\hat{f}^\dagger(t)]/2 , \tag{C3}$$

and $\hat{f}_i(\Omega)$ is that of

$$\hat{f}_i(t)\equiv[\hat{f}(t)e^{i\Delta\hat{\phi}(t)}-e^{-i\Delta\hat{\phi}(t)}\hat{f}^\dagger(t)]/2i . \tag{C4}$$

The correlation functions of $\hat{f}_r(t)$ and $\hat{f}_i(t)$ are

$$\langle\hat{f}_r(t)\hat{f}_r(u)\rangle=\langle\hat{f}_i(t)\hat{f}_i(u)\rangle=\delta(t-u)\tfrac{1}{2}(n_{th}+\tfrac{1}{2}) . \tag{C5}$$

Substituting (B13) into (C1), we obtain

$$\Delta\hat{r}_1(\Omega)=\frac{\{-A_3\tilde{F}_c+(A_1-i\Omega)[\hat{G}_r(\Omega)+\sqrt{\omega/Q_e}\hat{f}_r(\Omega)]\}}{A_2A_3+\Omega^2+i\Omega A_1}$$

$$-\hat{f}_r(\Omega)\ , \tag{C6}$$

where $\hat{G}_r(\Omega)$ is the Fourier transform of $\hat{G}_r(t)$, which is defined as

$$\hat{G}_r(t)\equiv\tfrac{1}{2}[\hat{G}(t)e^{i\Delta\hat{\phi}(t)}+e^{-i\Delta\hat{\phi}(t)}\hat{G}^{\dagger}(t)]\ . \tag{C7}$$

The correlation functions are

$$\langle\hat{G}_r(t)\hat{G}_r(u)\rangle=\delta(t-u)\frac{1}{2}\left[\frac{\omega}{Q_0}(n_{\rm th}+\tfrac{1}{2})+\tfrac{1}{2}(\langle\tilde{E}_{CV}\rangle+\langle\tilde{E}_{VC}\rangle)\right], \tag{C8}$$

and

$$\langle\hat{G}_r(t)\tilde{F}_c(u)\rangle=-\delta(t-u)\tfrac{1}{2}A_0(\langle\tilde{E}_{CV}\rangle+\langle\tilde{E}_{VC}\rangle)\ . \tag{C9}$$

The power spectrum $P_{\Delta\hat{r}_1}(\Omega)$ is then obtained as

$$P_{\Delta\hat{r}_1}(\Omega)=\left\{\frac{\omega}{Q_e}A_3^2P_{\tilde{F}_c}(\Omega)+\frac{\omega}{Q_e}(A_1^2+\Omega^2)P_{\hat{G}_r}(\Omega)+\left[\left[\frac{\omega}{Q_e}A_1-A_2A_3-\Omega^2\right]^2+\Omega^2\left[\frac{\omega}{Q_e}+A_1\right]^2\right]P_{\hat{f}_r}(\Omega)\right.$$
$$\left.-2A_1A_3\frac{\omega}{Q_e}\langle\tilde{F}_c(\Omega)\hat{G}_r(\Omega)\rangle\right\}\Big/[(A_2A_3+\Omega^2)^2+\Omega^2A_1^2]\ . \tag{C10}$$

Using correlation functions (3.37), (C8), (C5), and (C9), and approximations (4.3) and (4.5), $P_{\Delta\hat{r}_1}(\Omega)$ is calculated to be

$$P_{\Delta\hat{r}_1}(\Omega)=\tfrac{1}{2}\ , \tag{C11}$$

which is identical to (4.14).

Similarly, substitution of (B21) and (C2) leads to

$$\Delta\hat{\psi}(\Omega)=\frac{i}{\Omega A_0}\hat{G}_i(\Omega)+\frac{\Omega+i\omega/Q_e}{\Omega r_0}\hat{f}_i(\Omega)$$
$$+A_4\left[iA_2\frac{\hat{H}_r(\Omega)}{\Omega}-\tilde{F}_c(\Omega)\right]\Big/(A_2A_3+\Omega^2+i\Omega A_1)\ , \tag{C12}$$

where $\hat{G}_i(\Omega)$ is the Fourier transform of

$$\hat{G}_i(t)\equiv\frac{1}{2i}[\hat{G}(t)e^{i\Delta\hat{\phi}(t)}-e^{-i\Delta\hat{\phi}(t)}\hat{G}^{\dagger}(t)]\ . \tag{C13}$$

The correlation function of $\hat{G}_i(t)$ is the same as (C8). The power spectrum of $\Delta\hat{\psi}(t)$ is then obtained as

$$P_{\Delta\hat{\psi}}(\Omega)=\frac{1}{\Omega^2A_0^2}P_{\hat{G}_i}(\Omega)+\frac{\Omega^2+(\omega/Q_e)^2}{\Omega^2}P_{\hat{f}_i}(\Omega)$$
$$+A_4^2\left[\frac{A_2^2}{\Omega^2}P_{\hat{H}_r}(\Omega)+P_{\tilde{F}_c}(\Omega)\right]\Big/[(A_2A_3+\Omega^2)^2+\Omega^2A_1^2]\ , \tag{C14}$$

where

$$r_0=\sqrt{\omega/Q_e}A_0\ , \tag{C15}$$

is used. Using the correlation functions and the same approximations, (C15) becomes

$$P_{\Delta\hat{\psi}}(\Omega)=n_{\rm sp}(1+\alpha^2)\frac{\omega/Q}{\Omega^2A_0^2}+\frac{1}{2A_0^2\omega/Q_e}\ . \tag{C16}$$

If approximations $\alpha\ll1$ and $n_{\rm sp}\cong1$ are used, furthermore, (C17) reduces to (4.16).

## APPENDIX D

In this appendix, the *measured* photon-flux fluctuation operator in the QND measurement scheme is derived. The goal is Eq. (5.2), which relates the output photon-flux fluctuation $\Delta\hat{N}_1$ with the observed photon-flux fluctuation operator $\Delta\hat{N}_1^{\rm obs}$.

As is shown in Fig. 5, the output wave (signal wave) $\hat{r}_1$ and the probe wave $\hat{r}_p$ propagate in the optical Kerr medium interacting with each other. Here, $\hat{r}_p$ is the amplitude operator which is similarly normalized as $\hat{r}_1$, that is, $\hat{r}_p^{\dagger}\hat{r}_p$ expresses the photon flux of the probe wave as in

$$\hat{N}_p=\hat{r}_p^{\dagger}\hat{r}_p\ . \tag{D1}$$

The spatial evolution of $\hat{r}_1$ or $\hat{r}_p$ in the Kerr medium is described by Heisenberg's equation of motion using the interaction Hamiltonian of the optical Kerr effect as[21]

$$-i\frac{d}{dz}\hat{r}_p(z)=\kappa\hat{N}_1\hat{r}_p(z) \tag{D2}$$

and

$$-i\frac{d}{dz}\hat{r}_1(z)=\kappa\hat{N}_p\hat{r}_1(z)\ , \tag{D3}$$

where

$$\kappa\equiv\frac{\hbar\omega_p\omega\chi^{(3)}}{2\epsilon_0\epsilon c^2A}\ . \tag{D4}$$

Integration of (D2) and (D3) from $z=0$ to $L$ gives

$$\hat{r}_p(L)=\exp[i(F')^{1/2}\hat{N}_1]\hat{r}_p(0) \tag{D5}$$

and

$$\hat{r}_1(L)=\exp[i(F')^{1/2}\hat{N}_p]\hat{r}_1(0)\ , \tag{D6}$$

where $(F')^{1/2}$ is given as $\kappa L$. Since $\hat{r}_p^{\dagger}\hat{r}_p$ and $\hat{r}_1^{\dagger}\hat{r}_1$ are constants of motion in the transparent Kerr medium, the expansions for $\hat{r}_p$ and $\hat{r}_1$ are written instead of (4.12) as

$$\hat{r}_p(z)=r_{p0}e^{-i\hat{\phi}_p(z)} \tag{D7}$$

and

$$\hat{r}_1(z)=r_0e^{-i\hat{\psi}_1(z)}\ , \tag{D8}$$

where $r_{p0}$ is $\langle\hat{r}_p\rangle$. Substituting (D7) into (D5), and (D8) into (D6), we obtain

$$\hat{\phi}_p(L)=\hat{\phi}_p(0)-(F')^{1/2}\hat{N}_1 \tag{D9}$$

and

$$\hat{\psi}_1(L)=\hat{\psi}_1(0)-(F')^{1/2}\hat{N}_p\ . \tag{D10}$$

The phase sign is defined in this paper so that the negative sign denotes the phase delay (note that the sign is inversely defined in Ref. 21). Equation (D10) is rewritten as (5.5) with the notation $\hat{\psi}_1$ and $\hat{\psi}_2$ for the output phase operators before and after passage through the Kerr medium.

The balanced-mixer detector shown in Fig. 5 measures the observable $\cos[\hat{\phi}_p(L)-\hat{\phi}_{\rm ref}]$, where $\hat{\phi}_{\rm ref}$ is the phase of the reference wave passing through another arm.[21] For simplicity, $\hat{\phi}_p$ and $\hat{\phi}_{\rm ref}$ are redefined as those in front of beam splitter 2. Since $\hat{\phi}_p(L)-\hat{\phi}_{\rm ref}$ can be biased by an optical delay introduced in a reference arm so that $\langle\hat{\phi}_p(L)-\hat{\phi}_{\rm ref}\rangle=\pi/2$, $\cos[\hat{\phi}_p(L)-\hat{\phi}_{\rm ref}]$ is regarded as $\Delta\hat{\phi}_p(L)-\Delta\hat{\phi}_{\rm ref}$ when the fluctuation is small. We then define the observed photon-flux fluctuation operator $\Delta\hat{N}_1^{\rm obs}$ using $\Delta\hat{\phi}_p(L)-\Delta\hat{\phi}_{\rm ref}$ as

$$\Delta\hat{N}_1^{\rm obs}\equiv-[\Delta\hat{\phi}_p(L)-\Delta\hat{\phi}_{\rm ref}]/(F')^{1/2}\ . \tag{D11}$$

Substituting (D9) into (D11), we obtain

$$\Delta\hat{N}_1^{\rm obs}=\Delta\hat{N}_1-[\Delta\hat{\phi}_p(0)-\Delta\hat{\phi}_{\rm ref}]/(F')^{1/2}\ . \tag{D12}$$

When the transmission of beam splitter 1 is close to unity, the probe-wave photon flux passing through the Kerr medium is much smaller than that of the reference wave so that $\Delta\hat{\phi}_{\rm ref}$ can be negligible as compared with $\Delta\hat{\phi}_p(0)$,

$$\Delta\hat{N}_1^{\rm obs}=\Delta\hat{N}_1-\Delta\hat{\phi}_p(0)/(F')^{1/2}\ . \tag{D13}$$

## APPENDIX E

In this appendix, the amplitude and phase noise spectra of the *output wave with feedback* for the proposed scheme are obtained. Equations (6.2) and (6.5) are derived from (3.24), (3.25), (4.10), (4.11), (6.1), and (5.6).

The Fourier transforms of these equations are

$$i\Omega\,\Delta\hat{A}(\Omega)=A_3\,\Delta\tilde{N}_c(\Omega)+\hat{G}_r(\Omega)+\sqrt{\omega/Q_e}\,\hat{f}_r(\Omega)\ , \tag{E1}$$

$$i\Omega\,\Delta\hat{\phi}(\Omega)=A_4\Delta\tilde{N}_c(\Omega)+\frac{1}{A_0}\hat{G}_i(\Omega)+\sqrt{\omega/Q_e}\,\frac{1}{A_0}\hat{f}_i(\Omega)\ , \tag{E2}$$

$$\Delta\hat{r}_1(\Omega)=\sqrt{\omega/Q_e}\,\Delta\hat{A}(\Omega)-\hat{f}_r(\Omega)\ , \tag{E3}$$

$$\Delta\hat{\psi}_1(\Omega)=\Delta\hat{\phi}(\Omega)+\frac{1}{r_0}\hat{f}_i(\Omega)\ , \tag{E4}$$

$$i\Omega\,\Delta\tilde{N}_c(\Omega)=-h[2r_0\,\Delta\hat{r}_1(\Omega)-\Delta\hat{\phi}(\Omega)/(F')^{1/2}]+A_1\,\Delta\tilde{N}_c(\Omega)+A_2\,\Delta\hat{A}(\Omega)+\tilde{F}_c(\Omega)\ , \tag{E5}$$

and

$$\Delta\hat{\psi}_2(\Omega)=\Delta\hat{\psi}_1(\Omega)-(F')^{1/2}\Delta\hat{N}_p(\Omega)\ . \tag{E6}$$

Eliminating $\Delta\hat{A}(\Omega)$ and $\Delta\tilde{N}_c(\Omega)$ from (E1), (E3), and (E5) we obtain

$$\Delta\hat{r}_1(\Omega)=[B_1\hat{G}_r(\Omega)+B_2\tilde{F}_c(\Omega)+B_3\hat{f}_r(\Omega)+B_4]/B_5\ , \tag{E7}$$

where

$$B_1=\sqrt{\omega/Q_e}(1-i\Omega/A_1)\ , \tag{E8}$$

$$B_2=-\sqrt{\omega/Q_e}A_3/A_1\ , \tag{E9}$$

$$B_3=-A_2A_3/A_1+[(\omega/Q_e)-i\Omega](1-i\Omega/A_1)\ , \tag{E10}$$

$$B_4=-\sqrt{\omega/Q_e}hA_3\,\Delta\hat{\phi}_p/(F')^{1/2}A_1\ , \tag{E11}$$

and

$$B_5=A_2A_3/A_1+i\Omega(1-i\Omega/A_1)-\sqrt{\omega/Q_e}2r_0hA_3/A_1\ . \tag{E12}$$

The power spectrum of $\Delta\hat{r}_1(\Omega)$ is obtained from (E7) as

$$P_{\Delta\hat{r}_1}(\Omega)=\frac{B_1^*B_1P_{\hat{G}_r}(\Omega)+B_2^*B_2P_{\tilde{F}_c}(\Omega)+(B_1^*B_2+B_1B_2^*)\langle\hat{G}_r(\Omega)\tilde{F}_c(\Omega)\rangle+B_3^*B_3P_{\hat{f}_r}(\Omega)+\frac{\omega}{Q_e}\frac{A_3^2}{A_1^2}\frac{h^2}{F'}P_{\Delta\hat{\phi}_p}(\Omega)}{B_5^*B_5}\ . \tag{E13}$$

Using (E8)–(E12) and the correlation functions, and the assumption of an extremely high pumping level already used in Sec. IV, (E13) becomes

$$P_{\Delta\hat{r}_1}(\Omega)=\frac{\frac{1}{2}\left[\left[\frac{\omega}{Q_e}\right]^2+\Omega^2+\left[\frac{\omega}{Q_e}\right]^2\frac{h^2}{2F'r_0^2}P_{\Delta\hat{\phi}_p}(\Omega)\right]}{\left[\frac{\omega}{Q_e}\right]^2(1+h^2)+\Omega^2}\ . \tag{E14}$$

Since the QND measurement does not disturb the photon-flux fluctuation, $P_{\Delta\hat{r}_2}(\Omega)$ is also given by (E14), which leads to (6.2).

The phase noise spectrum is to be calculated in the same manner, which implies the elimination of $\Delta\hat{A}(\Omega)$, $\Delta\tilde{N}_c(\Omega)$, $\Delta\hat{\phi}(\Omega)$, and $\Delta\hat{r}_1(\Omega)$ from (E1)–(E5). The results are

$$\Delta\hat{\psi}_1(\Omega)=C_1\hat{G}_i(\Omega)+C_2\hat{f}_i(\Omega)+C_3\hat{G}_r(\Omega)+C_4\hat{f}_r(\Omega)+C_5\tilde{F}_c(\Omega)+C_6\Delta\hat{\phi}_p(\Omega) \tag{E15}$$

and

$$P_{\Delta\hat{\psi}_1}(\Omega)=C_1^*C_1P_{\hat{G}_i}(\Omega)+C_2^*C_2P_{\hat{f}_i}(\Omega)+C_3^*C_3P_{\hat{G}_r}(\Omega)+C_4^*C_4P_{\hat{f}_r}(\Omega)+C_5^*C_5P_{\tilde{F}_c}(\Omega)+(C_3^*C_5+C_5^*C_3)\langle\hat{G}_r(\Omega)\tilde{F}_c(\Omega)\rangle+C_6^*C_6P_{\Delta\hat{\phi}_p}(\Omega)\ , \tag{E16}$$

where

$$C_1\equiv 1/i\Omega A_0\ , \tag{E17}$$

$$C_2=(\sqrt{\omega/Q_e}+i\Omega/\sqrt{\omega/Q_e})/i\Omega A_0\ , \tag{E18}$$

$$C_3=\frac{1}{i\Omega}\left[-\frac{A_2}{A_1}+2h\frac{\omega A_3}{Q_eA_1}A_0\right]\frac{A_4}{B_5}\ , \tag{E19}$$

$$C_4=\frac{\sqrt{\omega/Q_e}}{i\Omega}\left[-\frac{A_2}{A_1}+2h\frac{\omega A_3}{Q_eA_1}A_0-i\Omega 2h\frac{A_3}{A_1}A_0\right]\frac{A_4}{B_5}\ , \tag{E20}$$

$$C_5=-\frac{A_4}{A_1B_5}\ , \tag{E21}$$

and

$$C_6=\frac{hA_4}{A_1B_5}\frac{1}{(F')^{1/2}}\ . \tag{E22}$$

If $\alpha=0$ (i.e., $A_4=0$) and an extremely high pumping level are assumed, the noise spectrum of $\Delta\hat{\psi}_2$ is obtained as

$$P_{\Delta\hat{\psi}_2}(\Omega)=\left[\frac{\omega}{Q_e}\right]^2\frac{1}{\Omega^2r_0^2}+\frac{1}{2r_0^2}+F'P_{\Delta\hat{N}_p}(\Omega)\ , \tag{E23}$$

which is the same as (6.5).


[1]H. Takahashi, Adv. Commun. Syst. **1**, 227 (1965).
[2]D. Stoler, Phys. Rev. D **4**, 1925 (1971).
[3]H. P. Yuen, Phys. Rev. A **13**, 2226 (1976).
[4]H. Brunet, Phys. Lett. **10**, 172 (1964).
[5]J. Harms and J. Lorigony, Phys. Lett. **10**, 173 (1964).
[6]H. P. Yuen and J. H. Shapiro, IEEE Trans. Info. Theory **IT-24**, 657 (1978).
[7]J. H. Shapiro, H. P. Yuen, and J. A. Machado Mata, IEEE Trans. Info. Theory **IT-25**, 179 (1979).
[8]H. P. Yuen and J. H. Shapiro, IEEE Trans. Info. Theory **IT-26**, 78 (1980).
[9]C. M. Caves, Phys. Rev. D **23**, 1693 (1981).
[10]R. Bondurant and J. H. Shapiro, Phys. Rev. D **30**, 2548 (1984).
[11]H. P. Yuen and J. H. Shapiro, Opt. Lett. **4**, 334 (1979).
[12]R. Bondurant, P. Kumar, J. H. Shapiro, and M. Maeda, Phys. Rev. A **30**, 343 (1984).
[13]R. E. Slusher, L. Hollberg, R. Yurke, J. C. Merts, and J. F. Valley, Phys. Rev. A **31**, 3512 (1985).
[14]M. Levenson, R. M. Shelby, A. Aspect, M. Reid, and D. F. Walls, Phys. Rev. A **32**, 1550 (1985).
[15]D. F. Walls, Nature **306**, 141 (1983).
[16]P. Carruthers and M. M. Neito, Rev. Mod. Phys. **40**, 411 (1968).
[17]R. Short and L. Mandel, Phys. Rev. Lett. **51**, 384 (1983).
[18]M. C. Teich and B. E. A. Saleh, J. Opt. Soc. Am. B **2**, 275 (1985).
[19]Y. Yamamoto *et al.*, US-Japan Seminar on Coherence, Incoherence and Chaos in Quantum Electronics, Nara, Japan, 1984 (unpublished); S. Machida and Y. Yamamoto, Opt. Commun. (to be published).
[20]H. A. Haus and Y. Yamamoto, Phys. Rev. A (to be published).
[21]N. Imoto, H. A. Haus, and Y. Yamamoto, Phys. Rev. A **32**, 2287 (1985).
[22]H. Haken, *Encyclopedia of Physics* (Springer-Verlag, Berlin, 1970), Vol. XXV/2c.
[23]M. Sargent III, M. O. Scully, and W. E. Lamb, Jr., *Laser Physics* (Addison-Wesley, Reading, Mass., 1974).
[24]M. Lax and W. H. Louisell, Phys. Rev. **185**, 568 (1969).
[25]R. J. Glauber, Phys. Rev. **131**, 2766 (1963).
[26]E. C. G. Sudarshan, Phys. Rev. Lett. **10**, 277 (1963).
[27]C. W. Gardinar and M. J. Collet, Phys. Rev. A **31**, 3761 (1985).
[28]H. A. Haus, *Waves and Fields in Optoelectronics* (Prentice-Hall, Englewood Cliffs, 1984); H. A. Haus and Y. Yamamoto, Phys. Rev. A **29**, 1261 (1984).
[29]Y. Yamamoto and N. Imoto, IEEE J. Quantum Electron. (to be published).
[30]O. Nilsson, Y. Yamamoto, and S. Machida, IEEE J. Quantum Electron. (to be published).
[31]W. H. Louisell, *Quantum Statistical Properties of Radiation* (Wiley, New York, 1973).
[32]H. Haug and H. Haken, Z. Phys. **204**, 262 (1967).
[33]H. Haug, Phys. Rev. **184**, 338 (1969).
[34]Y. Yamamoto, IEEE J. Quantum Electron. **QE-19**, 34 (1983).
[35]C. H. Henry, IEEE J. Quantum Electron. **QE-18**, 259 (1982).
[36]G. J. Milburn and D. F. Walls, Phys. Rev. A **28**, 2065 (1983).
[37]P.-L. Liu, L. E. Fencil, J.-S. Ko, I. P. Kaminow, T. P. Lee, and C. A. Burrus, IEEE J. Quantum Electron. **QE-19**, 1348 (1983).
[38]E. Jakeman and E. R. Pike, J. Phys. A **1**, 128 (1968).
[39]H. P. Yuen and V. W. S. Chan, Opt. Lett. **8**, 177 (1983).
[40]E. Arthurs and J. L. Kelly, Jr., Bell Syst. Tech. J. **44**, 725 (1965).
[41]C. M. Caves, K. S. Thorne, R. W. P. Drever, V. D. Sandberg, and M. Zimmerman, Rev. Mod. Phys. **52**, 341 (1980).